JCB Journal of Cell Biology

ARTICLE

Kindlin-2 regulates mesenchymal stem cell differentiation through control of YAP1/TAZ

Ling Guo[1], Ting Cai[1], Keng Chen[1], Rong Wang[1], Jiaxin Wang[1], Chunhong Cui[1], Jifan Yuan[1], Kuo Zhang[1], Zhongzhen Liu[1], Yi Deng[1], Guozhi Xiao[1,2], and Chuanyue Wu[1,3]

Precise control of mesenchymal stem cell (MSC) differentiation is critical for tissue development and regeneration. We show here that kindlin-2 is a key determinant of MSC fate decision. Depletion of kindlin-2 in MSCs is sufficient to induce adipogenesis and inhibit osteogenesis in vitro and in vivo. Mechanistically, kindlin-2 regulates MSC differentiation through controlling YAP1/TAZ at both the transcript and protein levels. Kindlin-2 physically associates with myosin light-chain kinase in response to mechanical cues of cell microenvironment and intracellular signaling events and promotes myosin light-chain phosphorylation. Loss of kindlin-2 inhibits RhoA activation and reduces myosin light-chain phosphorylation, stress fiber formation, and focal adhesion assembly, resulting in increased Ser127 phosphorylation, nuclear exclusion, and ubiquitin ligase atrophin-1 interacting protein 4–mediated degradation of YAP1/TAZ. Our findings reveal a novel kindlin-2 signaling axis that senses the mechanical cues of cell microenvironment and controls MSC fate decision, and they suggest a new strategy to regulate MSC differentiation, tissue repair, and regeneration.

Introduction

Mesenchymal stem cells (MSCs) are capable of differentiating into multiple cell lineages, including osteoblasts and adipocytes, in response to environment cues (Watt and Hogan, 2000; Bianco et al., 2001; Li et al., 2016). The commitment of MSCs to different cell lineages is normally precisely controlled (Bianco et al., 2001; McBeath et al., 2004; Engler et al., 2006; Li et al., 2016), and dysregulation of this process is often associated with various pathological conditions (Valenti et al., 2016). For example, MSCs can differentiate into either osteoblasts or adipocytes, and alteration of osteogenic and adipogenic differentiation is a causal factor in the development of many human bone diseases (James, 2013; Jing et al., 2016). In particular, increased marrow adiposity has been observed in most bone loss conditions including aging (Justesen et al., 2001; Moerman et al., 2004) and various pathological conditions (Bredella et al., 2011; Cao, 2011; Cohen et al., 2012; Georgiou et al., 2012; Misra and Klibanski, 2013; Chen et al., 2016). Therefore, restoration of MSC cell lineage commitment is an appealing therapeutic strategy for many human bone diseases (Chen et al., 2016; Jing et al., 2016).

A large body of experimental evidence suggests that an inverse correlation exists between adipogenesis and osteogenesis (James, 2013). The commitment and differentiation of MSCs toward an adipogenic or osteogenic cell fate depend on the MSC microenvironment (Bianco et al., 2001; Chen et al., 2016; Li et al., 2016). In particular, adhesive and mechanical cues play critical roles in control of MSC fate decision. Recent studies suggest that YAP1 and TAZ are key signaling intermediates that link adhesive and mechanical cues to MSC differentiation (McBeath et al., 2004; Dupont et al., 2011; Hiemer and Varelas, 2013; Zhong et al., 2013). They regulate cell proliferation and survival and play important roles in controlling organ growth, stem cell self-renewal and cell differentiation (Dupont, 2016). In addition, RhoA is considered as an integral component of mechanosensing: RhoA promotes actin polymerization and actomysin contraction, and it sustains focal adhesion maturation (Saltiel, 2003; Sordella et al., 2003; McBeath et al., 2004).

Although it has been well documented that adhesive and mechanical cues can control MSC differentiation (McBeath et al., 2004; Engler et al., 2006; Dupont et al., 2011), Yap/Taz activators that can sense adhesive and mechanical cues and regulate MSC differentiation remain to be clarified. Kindlin-2 is an important integrin- and actin-binding protein that has been implicated in regulation of actin cytoskeleton and integrin bidirectional signaling (Tu et al., 2003; Shi et al., 2007; Larjava et al., 2008; Ma et al., 2008; Montanez et al., 2008; Qu et al., 2011, 2014; Bledzka et al., 2016; Li et al., 2017). Global deletion of kindlin-2

[1]Guangdong Provincial Key Laboratory of Cell Microenvironment and Disease Research, Shenzhen Key Laboratory of Cell Microenvironment, and Department of Biology, Southern University of Science and Technology, Shenzhen, China; [2]Department of Biochemistry, Rush University Medical Center, Chicago, IL; [3]Department of Pathology, University of Pittsburgh School of Medicine, Pittsburgh, PA.

Correspondence to Chuanyue Wu: wucy@sustc.edu.cn.

in mice results in periimplantation lethality because of extensive detachment of the endoderm and epiblasts (Dowling et al., 2008; Montanez et al., 2008), demonstrating a critical role of kindlin-2 in early embryonic development. Recently, using a conditional knockout strategy, we have demonstrated that kindlin-2 is critical for skeletal development (Wu et al., 2015). Ablation of kindlin-2 in paired related homeobox 1 (Prx1)–expressing mesenchymal progenitors in mice causes severe limb shortening and neonatal lethality, probably at least in part because of loss of the skull vault and chondrodysplasia (Wu et al., 2015). Although it is clear that kindlin-2 is critical for skeletal development, whether or not kindlin-2 functions in the control of MSC commitment and differentiation into different cell lineages and the underlying mechanism are not clear. In the current study, we have used a combination of in vitro and in vivo approaches to determine the functions and the mechanism of kindlin-2 in MSC differentiation. We have found that loss of kindlin-2 in MSCs induces drastic and spontaneous adipocyte differentiation and inhibits osteogenic differentiation. Mechanistically, we have identified YAP1/TAZ as key downstream effectors of kindlin-2 signaling in control of MSC differentiation. Loss of kindlin-2 in MSCs dramatically reduced the mRNA and protein levels of YAP1/TAZ, whereas forced expression of YAP1 or TAZ in kindlin-2–deficient MSCs restored the capability of MSC differentiation into osteogenic cells. At the molecular level, kindlin-2 physically associates with myosin light-chain kinase (MLCK) in response to mechanical cues of cell microenvironment (e.g., substrate stiffness) and intracellular signaling events (e.g., RhoA activation) and promotes myosin light-chain phosphorylation. Loss of kindlin-2 inhibits RhoA activation and reduces myosin light-chain phosphorylation, stress fiber formation, and focal adhesion assembly, resulting in increased Ser127 phosphorylation, nuclear exclusion, and atrophin-1 interacting protein 4 (AIP4)–mediated degradation of YAP1/TAZ. Our findings reveal a novel kindlin-2 signaling axis that controls MSC fate decision and suggest a new strategy to regulate MSC differentiation, tissue repair, and regeneration.

Results

Kindlin-2 controls cell fate decision of MSCs

To begin investigating the role of kindlin-2 in regulation of MSC differentiation, we first analyzed the level of kindlin-2 expression during osteogenic or adipogenic differentiation of MSCs derived from human placenta, which are known to have multilineage differentiation potential (Fukuchi et al., 2004; Li et al., 2011). The results showed that both the protein (Fig. 1, A and B) and transcript (Fig. 1 C) levels of kindlin-2 were markedly increased during osteogenic differentiation. In contrast, both the protein and transcript levels of kindlin-2 were reduced during adipogenic differentiation (Fig. 1, A–C). These results were confirmed by immunofluorescence staining of human MSCs (hMSCs) that were undergoing osteogenic or adipogenic differentiations (Fig. S1 A). To further this, we analyzed the expression of kindlin-2 in mouse femur bone sections by immunohistochemistry. Consistent with the results of the in vitro studies described above, cells with high levels of kindlin-2 expression were readily detected in trabecular bone (adjacent to the growth plate, surrounding the areas of bone formation) and cortical bone, whereas adipose cells in the femur bone marrow cavity express much lower levels of kindlin-2 (Fig. S1 B). Collectively, these results demonstrate that the level of kindlin-2 is significantly changed during MSC differentiation; it increases during osteogenic differentiation and decreases during adipogenic differentiation.

We next tested whether the change of kindlin-2 level is functionally important to adipogenic and osteogenic differentiation of MSCs. To do this, we knocked down kindlin-2 in hMSCs by RNAi and analyzed the effects on MSC differentiation. The reduction of the level of kindlin-2 but not that of kindlin-1 or -3 in the knockdown cells was confirmed by Western blotting (Fig. 1 D). Remarkably, depletion of kindlin-2 in hMSCs induced spontaneous adipogenic differentiation as demonstrated by strong staining of the cells with Oil Red O (Fig. 1, E and F). Reexpression of kindlin-2 in the kindlin-2 knockdown hMSCs effectively reversed adipogenic differentiation (Fig. 1, E and F). Consistent with this, expression of nuclear receptor peroxisome proliferator-activated receptor γ (PPARγ), a key transcription factor for adipogeneic differentiation, was significantly increased after removal of kindlin-2 (Fig. 1 G). Again, the increase of PPARγ was reversed by reexpression of kindlin-2 in the kindlin-2 knockdown hMSCs (Fig. 1 G). These results indicate that reduced expression of kindlin-2 is sufficient to induce spontaneous adipogenic differentiation of MSCs, providing initial evidence suggesting that kindlin-2 is functionally important for control of MSC differentiation. Depletion of kindlin-2 from hMSCs also reduced the rate of proliferation (Fig. S1, C and D) and increased the rate of apoptosis (Fig. S1 E).

To further test the function of kindlin-2 in MSC differentiation, we cultured kindlin-2 knockdown hMSCs and control hMSCs in adipogenic differentiation-induction and osteogenic differentiation-induction media, respectively. Although control hMSCs began to undergo adipogenic differentiation after they were cultured for 14 d under adipogenic conditions, kindlin-2 knockdown hMSCs were fully differentiated into adipocytes under the same condition as revealed by much stronger Oil Red O staining and a higher expression level of PPARγ compared with those of the control hMSCs (Fig. 1, H [top], I, and J). These results confirm that loss of kindlin-2 promotes MSC adipogenic differentiation. By marked contrast, whereas control hMSCs were readily differentiated into osteocytes after being cultured in the osteogenic differentiation medium for 14 d as revealed by strong Alizarin Red staining, kindlin-2 knockdown hMSCs failed to do so (Fig. 1, H [bottom] and K). Consistent with this, the expression levels of osteogenic differentiation markers such as osteoprotegerin (OPG) were dramatically decreased in kindlin-2 knockdown hMSCs compared with those in control hMSCs (Fig. 1 L), suggesting that kindlin-2 is critical for permitting osteogenic differentiation of MSCs.

We next investigated the function of kindlin-2 in regulation of osteogenesis and adipogenesis in vivo. Two experimental approaches were used. First, we ablated kindlin-2 in mesenchymal progenitors that express Prx1, a transcription factor that is expressed early during limb-bud mesoderm development (Cretekos et al., 2008), by crossing kindlin-2$^{fl/fl}$ mice with Prx1-Cre mice. Consistent with our recent studies (Wu et al., 2015), ablation

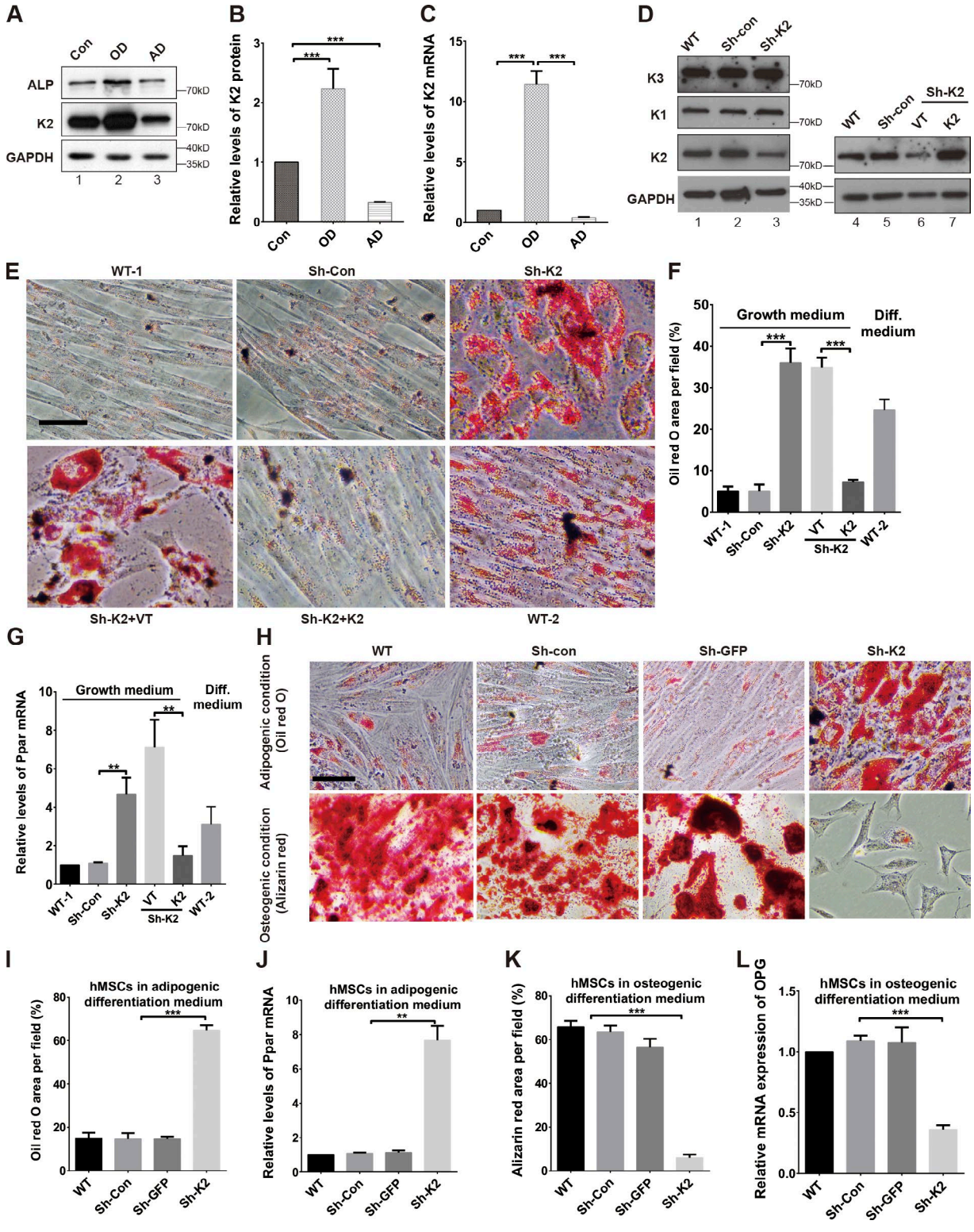

Figure 1. **Depletion of kindlin-2 promotes MSC adipogenic differentiation and inhibits osteogenic differentiation. (A–C)** hMSCs were cultured under control (Con; lane 1), osteogenic differentiation (OD; lane 2), or adipogenic differentiation (AD; lane 3) medium for 14 d. The cells were then analyzed by Western blotting with antibodies recognizing ALP, kindlin-2 (K2), and GAPDH (as a loading control; A). Protein levels of kindlin-2 relative to that of GAPDH in OD and AD medium were quantified by densitometry and compared with that in control medium (normalized to 1; mean ± SEM; $n = 3$; ***, $P < 0.001$; B). The mRNA levels of kindlin-2 in OD and AD medium were analyzed by RT-PCR and compared with those in control medium (normalized to 1). Bars represent means ± SEM; $n = 3$; ***, $P < 0.001$(C). **(D–G)** hMSCs were infected with control lentivirus (Sh-Con) or kindlin-2 shRNA lentivirus (Sh-K2). 2 d after the infection, the kindlin-2 shRNA lentivirus infectants were infected with a control vector lacking kindlin-2 sequence (Sh-K2+VT) or Plvx-K2, a lentiviral expression vector encoding WT kindlin-2 (Sh-K2+K2) for 3 d as described in Materials and methods. WT (WT-1), Sh-K2+VT, or Sh-K2+K2 hMSCs (as indicated in the figure) were cultured in normal culture

of kindlin-2 in Prx1-expressing mesenchymal progenitors in mice caused severe limb shortening and defective osteogenesis. Interestingly, defective osteogenesis is found not only in the cranial tissues but also throughout the skeleton of kindlin-2$^{fl/fl}$/Prx1-Cre mice (Fig. S2, A and B). The expression of osteogenic markers (i.e., Runt-related transcription factor 2 [Runx2], Osterix/Specificity protein-7 transcription factor [SP7], alkaline phosphatase [ALP], and bone γ-carboxyglutamate protein [BGLAP]) was significantly reduced (Fig. 2 A), whereas the expression of adipogenic genes (i.e., adiponectin, fatty acid–binding protein 4 [Fabp4], PPAR, and CCAAT/enhancer-binding protein α [Cebpa]) was significantly increased (Fig. 2 B) in response to loss of kindlin-2 in vivo. In the second approach, we transplanted GFP-labeled kindlin-2–deficient hMSCs and control hMSCs (Fig. 2 C), respectively, into nude mice and analyzed their ability to undergo osteogenic and adipogenic differentiation. The results showed that depletion of kindlin-2 inhibited osteogenesis and promoted adipogenesis, as indicated by the reduced expression of ALP (Fig. 2, D and E) and increased staining of perilipin (Fig. 2, F and G), an adipocyte-specific marker, in transplanted GFP-labeled kindlin-2–deficient hMSCs. Collectively, these results provide strong evidence for a critical role of kindlin-2 in control of cell fate decision of MSC in vivo (i.e., it promotes osteogenic differentiation whereas it inhibits adipogenic differentiation in vivo).

Kindlin-2 regulates YAP1 and TAZ in vitro and in vivo

We next sought to determine the molecular mechanism by which kindlin-2 controls cell fate determination of MSCs. We observed that, like the level of kindlin-2 (Fig. 1, A–C), the levels of YAP1 and TAZ, which are known to play a critical role in regulation of MSC lineage commitment (Karystinou et al., 2015) were also increased during hMSC osteogenic differentiation and reduced during hMSC adipogenic differentiation (Fig. S3, A–E). To further investigate this, we analyzed the expression of YAP1/TAZ in mouse femur bone sections. Immunohistochemistry showed that YAP1/TAZ-positive cells were abundantly detected in trabecular bone (adjacent to the growth plate, surrounding the areas of bone formation) and cortical bone, whereas YAP1/TAZ were undetectable in adipose cells of femur bone-marrow cavity (Fig. S3 F), which is reminiscent of the expression pattern of kindlin-2 (Fig. S1 B).

The correlation between the level of kindlin-2 and those of YAP1/TAZ raised a possibility that kindlin-2 may play an important role in control of the levels of YAP1/TAZ. To test this, we analyzed the effect of depleting kindlin-2 on YAP1/TAZ in hMSCs. The results showed that the levels of YAP1 and TAZ were indeed significantly reduced in kindlin-2 knockdown hMSCs compared with those in control hMSCs (Fig. 3, A, C, and D). To further test this, we infected MSCs isolated from kindlin-2$^{fl/fl}$ mice with adenovirus encoding Cre (Ad-Cre) or that encoding Laz (Ad-Laz) as a control. Western blotting showed that the level of kindlin-2 in the cells infected with Ad-Cre, but not those infected with Ad-Laz, was dramatically reduced (Fig. 3 J). Importantly, consistent with the results obtained with shRNA-mediated knockdown studies, both the mRNA (Fig. 3 I) and protein (Fig. 3, J and K) levels of YAP1/TAZ were significantly reduced in kindlin-2 knockout mouse MSCs.

Next, we reexpressed kindlin-2 in kindlin-2–deficient hMSCs and found that it markedly reversed the downregulation of YAP1/TAZ induced by the knockdown of kindlin-2 (Fig. 3, B–D). To further investigate this, we analyzed the levels of YAP1 and TAZ mRNAs by real-time RT-PCR. The results showed that they were also significantly reduced in kindlin-2 knockdown hMSCs (Fig. 3, E and F). Again, reexpression of kindlin-2 in kindlin-2–deficient hMSCs reversed the downregulation of YAP1/TAZ mRNAs induced by the knockdown of kindlin-2 (Fig. 3, E and F). Additionally, knockdown of kindlin-2 inhibited the nuclear localization of YAP1/TAZ (Fig. 3, G and H). Reexpression of kindlin-2 in kindlin-2–deficient hMSCs restored the nuclear localization of YAP1/TAZ (Fig. 3, G and H). Taken together, these results suggest that (1) kindlin-2 is critical for control of YAP1/TAZ and (2) kindlin-2 functions in this process by participating in regulation of both the mRNAs and proteins of YAP1/TAZ.

We next tested whether kindlin-2 regulates YAP1 and TAZ in vivo. To do this, we quantified the levels of YAP1 and TAZ mRNA derived from the femur tissues of the conditional kindlin-2 knockout mice (kindlin-2$^{fl/fl}$/Prx1-Cre mice) and the control mice (kindlin-2$^{fl/fl}$ mice), respectively. The results showed that the YAP1 and TAZ mRNA levels in the conditional kindlin-2 knockout mice were significantly reduced compared with those in the control mice (Fig. 3, L and M). Moreover, the protein levels of YAP1 and TAZ were also significantly reduced in the conditional kindlin-2 knockout mice compared with those in the control mice (Fig. 3, N–P). To further investigate this, we analyzed the levels of YAP1 and TAZ in mouse humeral bone sections by immunohistochemistry. Abundant YAP1 and TAZ were detected in the growth plate, surrounding the areas of bone formation in the control mice, whereas YAP1 and TAZ were undetectable in those of the conditional kindlin-2 knockout mice (Fig. S3 G). Collectively, these results confirm a critical role of kindlin-2 in regulation of YAP1 and TAZ in vivo.

medium for 14 d and analyzed by Western blotting with antibodies recognizing kindlin-1(K1), kindlin-2 (K2), kindlin-3 (K3), and GAPDH (as a loading control; D). Cells were stained with Oil Red O. Additionally, as a positive control WT hMSCs (WT-2) were cultured in adipogenic differentiation medium (diff. medium) for 14 d and stained with Oil Red O (E). Bar, 50 µm. The total areas of Oil Red O–positive staining per macroscopic field were quantified by using ImageJ (F). Data are means ± SEM; ***, P < 0.001 (n = 3). The mRNA levels of adipogenic markers (Ppar) in the kindlin-2 knockdown cells were analyzed by RT-PCR and compared with those of the control cells (normalized to 1; G). Data are means ± SEM; **, P < 0.01 (n = 3). **(H–L)** WT or infected hMSCs were cultured under adipogenic or osteogenic medium for 14 d. The cells were then stained with Oil Red O (top) or Alizarin Red S (bottom) as indicated in the figure (H). Bar, 50 µm. The total areas of Oil Red O staining per macroscopic field (I) and those of Alizarin Red S staining per macroscopic field (K) were quantified by using ImageJ. Data are means ± SEM; n = 3; ***, P < 0.001. The levels of mRNAs of adipogenic marker Ppar (J) or osteogenic marker OPG (L) in the cells were analyzed by RT-PCR and compared with those of the WT control cells (normalized to 1). Data are means ± SEM; **, P < 0.01; ***, P < 0.001 (n = 3).

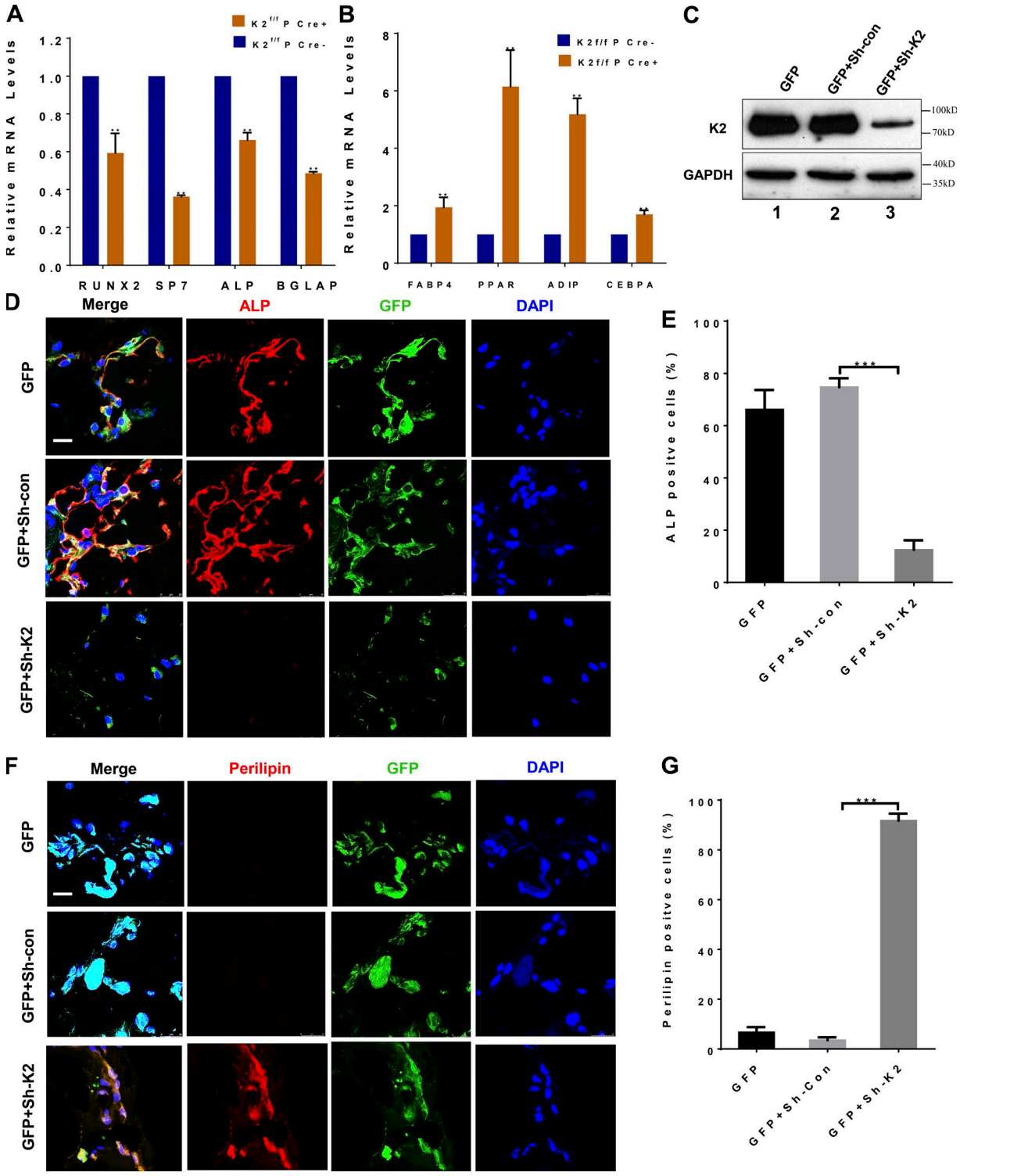

Figure 2. **kindlin-2 regulates osteogenesis and adipogenesis in vivo. (A and B)** Total RNAs were extracted from the femur tissues of the Prx1-Cre kindlin-$2^{fl/fl}$ newborn mice ($K2^{f/f}$ P Cre+) or Cre-negative kindlin-$2^{fl/fl}$ ($K2^{f/f}$ P Cre-) newborn mice. The levels of mRNAs of osteogenic markers (Runx2, SP7, ALP, and Bglap; A) and adipogenic markers (Fabp4, Ppar, adiponectin, and Cebpa; B) in the femur tissues of the Prx1-Cre kindlin-$2^{fl/fl}$ newborn mice ($K2^{f/f}$ P Cre+) were analyzed by RT-PCR and compared with those in the femur tissues of the kindlin-$2^{fl/fl}$ newborn mice ($K2^{f/f}$ P Cre-; normalized to 1). Data are means ± SEM; **, $P < 0.01$ (n = 3 mice). **(C–G)** GPF lentivirus–infected hMSCs (GFP; lane 1), control shRNA lentivirus-infected GFP hMSCs (GFP+Sh-Con; lane 2), and kindlin-2 shRNA lentivirus infected GFP hMSCs (GFP+Sh-K2; lane 3) were transplanted into the nude mice. Proteins were extracted from the transplants and were analyzed by Western blotting with antibodies to kindlin-2 or GAPDH (as a loading control; C). Immunostaining of the transplant sections with DAPI and ALP (D) or perilipin (F) antibody was performed 4 wk after transplantation. Bars, 50 µm. The percentages of ALP-positive (E) or perilipin-positive (G) hMSCs among total hMSCs are quantified by using ImageJ. Data are means ± SEM; n = 3 mice with three or four sections per mouse; ***, $P < 0.001$. More than 50 cells were counted in each panel.

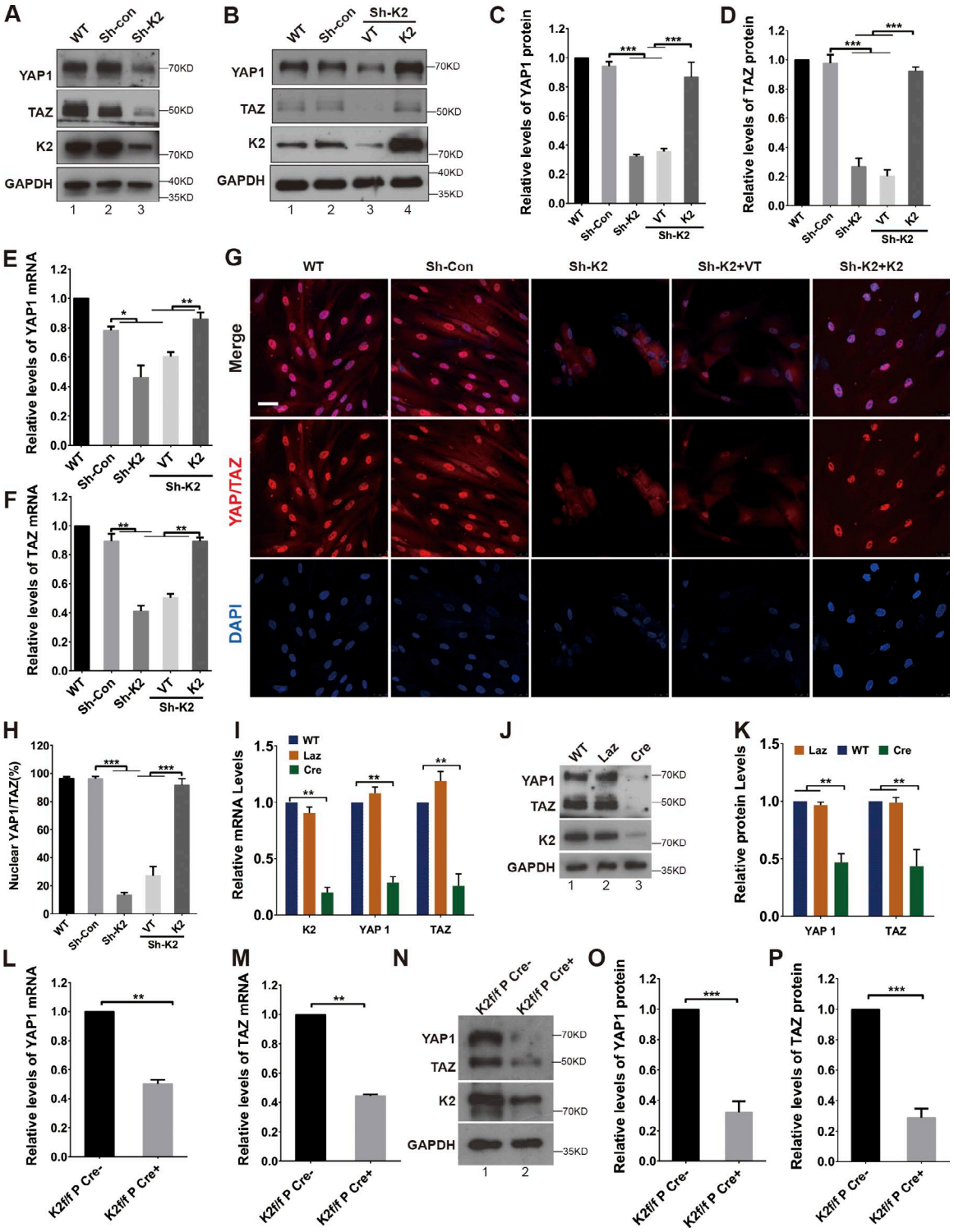

Figure 3. **kindlin-2 regulates YAP1 and TAZ at both the transcript and protein levels. (A–H)** hMSCs were infected with kindlin-2 shRNA or control lentivirus. 2 d after the infection, the kindlin-2 shRNA lentivirus infectants were transfected with a pLVX expression vector encoding kindlin-2 that is resistant to kindlin-2 shRNA lentivirus (K2) or a pLVX control vector lacking kindlin-2 coding sequence (VT). The cells were analyzed by Western blotting with antibodies as indicated (A and B). Protein levels of YAP1 (C) and TAZ (D) relative to that of GAPDH in infected cells were quantified by densitometry and compared with that of WT hMSCs (normalized to 1). Data are means ± SEM; $n = 3$; ***, $P < 0.001$. The mRNA levels of YAP1 (E) and TAZ (F) in the infected cells were analyzed by RT-PCR and compared with those in the WT cells (normalized to 1). The bars represent means ± SEM; $n = 3$; *, $P < 0.05$; **, $P < 0.01$. The cells were immunofluorescently stained with DAPI and YAP1/TAZ antibodies (G). Bar, 50 µm. The percentages of nuclear YAP/TAZ-positive cells among total cells were quantified (H). Data are means ± SEM; $n = 3$; ***, $P < 0.001$. At least 100 cells were counted in each experiment. **(I–K)** mMSCs isolated from kindlin-2$^{fl/fl}$ mice bone matrix were infected with Cre or Laz adenovirus. 3 d after the infection, the mRNA levels of kindlin-2, YAP1, and TAZ in the infected cells were analyzed by RT-PCR and compared with those in the WT cells (normalized to 1; I). The bars represent means ± SEM; $n = 3$; **, $P < 0.01$. The cells were analyzed by Western blotting

YAP1/TAZ mediate kindlin-2 regulation of MSC differentiation

The finding that kindlin-2 regulates YAP1 and TAZ raised the possibility that kindlin-2 controls MSC differentiation through YAP1 and TAZ. Similar to the effect of kindlin-2 knockdown on MSC differentiation (Fig. 1 A), knockdown of YAP1 was sufficient to induce spontaneous adipogenic differentiation (Fig. 4, A–D). To further test this, we increased the expression of YAP1 and TAZ, respectively, in kindlin-2 knockdown hMSCs, which expressed much lower levels of YAP1 and TAZ compared with control hMSCs (Fig. 4, E and F, compare lane 3 with lanes 1 and 2), by infecting the cells with lentiviral YAP1 or TAZ expression vector. The increase of YAP1 or TAZ level, but not that of kindlin-2, in the correspondent YAP1 or TAZ infectants was confirmed by Western blotting (Fig. 4, E and F, lane 4). Importantly, the forced increase of YAP1 or TAZ expression in kindlin-2–deficient hMSCs restored to a large extent the ability of MSCs to differentiate into osteocytes and reversed the adipogenic differentiation induced by the loss of kindlin-2 (Fig. 4, G–K). These results suggest that kindlin-2 controls MSC differentiation primarily through regulation of YAP1 and TAZ.

Both integrin- and actin-binding are involved in kindlin-2–mediated regulation of YAP1/TAZ and MSC differentiation

It has been well established that kindlin-2, through its F3 subdomain, interacts with integrins and regulates their activation (Shi et al., 2007; Larjava et al., 2008; Ma et al., 2008; Montanez et al., 2008; Qu et al., 2011, 2014; Bledzka et al., 2016). To test whether integrin-binding is involved in kindlin-2–mediated regulation of YAP1/TAZ and MSC differentiation, we expressed kindlin-2 bearing the QW615/AA mutation, which reduces the interaction with integrins (Shi et al., 2007), and WT kindlin-2, respectively, in kindlin-2–deficient hMSCs. Consistent with previous studies (Shi et al., 2007; Larjava et al., 2008; Ma et al., 2008; Montanez et al., 2008; Qu et al., 2011, 2014; Bledzka et al., 2016), knockdown of kindlin-2 (Fig. 5 A, lane 3) inhibited β1 integrin activation (Fig. 5 B). Whereas reexpression of WT kindlin-2 in kindlin-2–deficient hMSCs completely restored β1 integrin activation, reexpression of the integrin-binding defective QW615/AA mutant in kindlin-2–deficient hMSCs only modestly increased β1 integrin activation (Fig. 5, A and B). Similarly, whereas reexpression of WT kindlin-2 in kindlin-2–deficient hMSCs almost completely reversed the down-regulation of YAP1/TAZ mRNA and protein levels induced by the knockdown of kindlin-2, reexpression of the integrin-binding defective QW615/AA mutant did not increase YAP1/TAZ mRNA levels (Fig. 5, G and H) and only modestly increased YAP1/TAZ protein levels (Fig. 5, E and F).

In addition to interacting with integrins, kindlin-2 can interact with actin, and the latter interaction is mediated by the N-terminal most F0 domain of kindlin-2 (Bledzka et al., 2016). Consistent with previous studies (Bledzka et al., 2016), substitution of LK47 within F0 with AA inhibited the actin-binding activity of kindlin-2 (Fig. 5 C, compare lane 3 with 4). GFP-tagged LK47/AA mutants in hMSCs, like GFP-kindlin-2, were localized to focal adhesions where abundant vinculin was present (Fig. S4). To test the role of actin-binding on kindlin-2–mediated regulation of YAP1/TAZ, we expressed the actin-binding defective LK47/AA mutant and WT kindlin-2, respectively, in kindlin-2 knockdown hMSCs and determined the effects on YAP1/TAZ. The results showed that reexpression of the LK47/AA mutant, unlike that of WT kindlin-2, failed to reverse the down-regulation of YAP1/TAZ mRNA and protein levels induced by the loss of kindlin-2 (Fig. 5, D–H). Collectively, these results suggest that both integrin- and actin-binding are involved in kindlin-2–mediated regulation of YAP1 and TAZ.

Next, we assessed the roles of integrin- and actin-binding in kindlin-2 regulation of MSC differentiation. To do this, we reexpressed WT kindlin-2, actin-binding defective LK47/AA mutant, and integrin-binding defective QW615/AA mutant, respectively, in kindlin-2–deficient hMSCs and assessed their abilities to undergo adipogenic and osteogenic differentiation. The results showed that the actin-binding defective LK47/AA mutant and integrin-binding defective QW615/AA were much less effective in suppression of adipogenic differentiation and restoration of osteogenic differentiation than WT kindlin-2 (Fig. 5, I–M). It is worth noting, however, that reexpression of QW615/AA mutant did modestly increase osteogenic differentiation and partially reverse adipogenic differentiation (Fig. 5, I–M), indicating that the QW615/AA mutant may retain low levels of osteogenic-promoting and adipogenic-suppressing activities. This is consistent with a modest effect of reexpression of QW615/AA mutant on restoration of the levels of YAP1/TAZ (Fig. 5, A and E–H), providing additional evidence that kindlin-2 regulates MSC differentiation through controlling the levels of YAP1/TAZ.

Kindlin-2 regulates MSC geometry, actin stress fiber, and focal adhesion formation

Given the critical role of YAP/TAZ in mediating the effects of kindlin-2 on MSC differentiation, we next sought to determine the mechanism by which kindlin-2 regulates YAP1/TAZ. YAP1 and TAZ are known to be regulated by the actin cytoskeleton (Dupont et al., 2011; Halder et al., 2012; Aragona et al., 2013). We noted that kindlin-2–deficient hMSCs were smaller and often rounded compared with control hMSCs (Fig. 6, A–C; and Fig. S5). Furthermore, although hMSCs expressing a normal level of kindlin-2 formed extensive actin stress fibers and numerous focal adhesions, knockdown of kindlin-2 markedly reduced the numbers

with antibodies as indicated (J). Protein levels of YAP1 and TAZ (K) relative to that of GAPDH in infected cells were quantified by densitometry and compared with that of WT hMSCs (normalized to 1). Data are means ± SEM; $n = 3$; **, $P < 0.01$ (K). **(L–P)** The levels of YAP1 (L) and TAZ (M) mRNAs in the femur tissues of the kindlin-$2^{fl/fl}$ Prx1-Cre mice ($K2^{f/f}$ P Cre+) were analyzed by RT-PCR and compared with those of the Cre-negative kindlin-$2^{fl/fl}$ mice ($K2^{f/f}$ P Cre-; normalized to 1). Data are means ± SEM; **, $P < 0.01$; $n = 3$. Protein extracts from femur tissues of Cre-negative kindlin-$2^{fl/fl}$ mice (lane 1) and Prx1-Cre; kindlin-$2^{fl/fl}$ mice (lane 2) were analyzed by Western blotting with antibodies recognizing YAP1, TAZ, kindlin-2, or GAPDH (as a loading control; N). Protein levels of YAP1 (O) and TAZ (P) relative to that of GAPDH in tissues derived from the Prx1-Cre; kindlin-$2^{fl/fl}$ newborn mice were quantified by densitometry and compared with those from the Cre-negative kindlin-$2^{fl/fl}$ newborn mice (normalized to 1). The bars represent means ± SEM; $n = 3$; ***, $P < 0.001$.

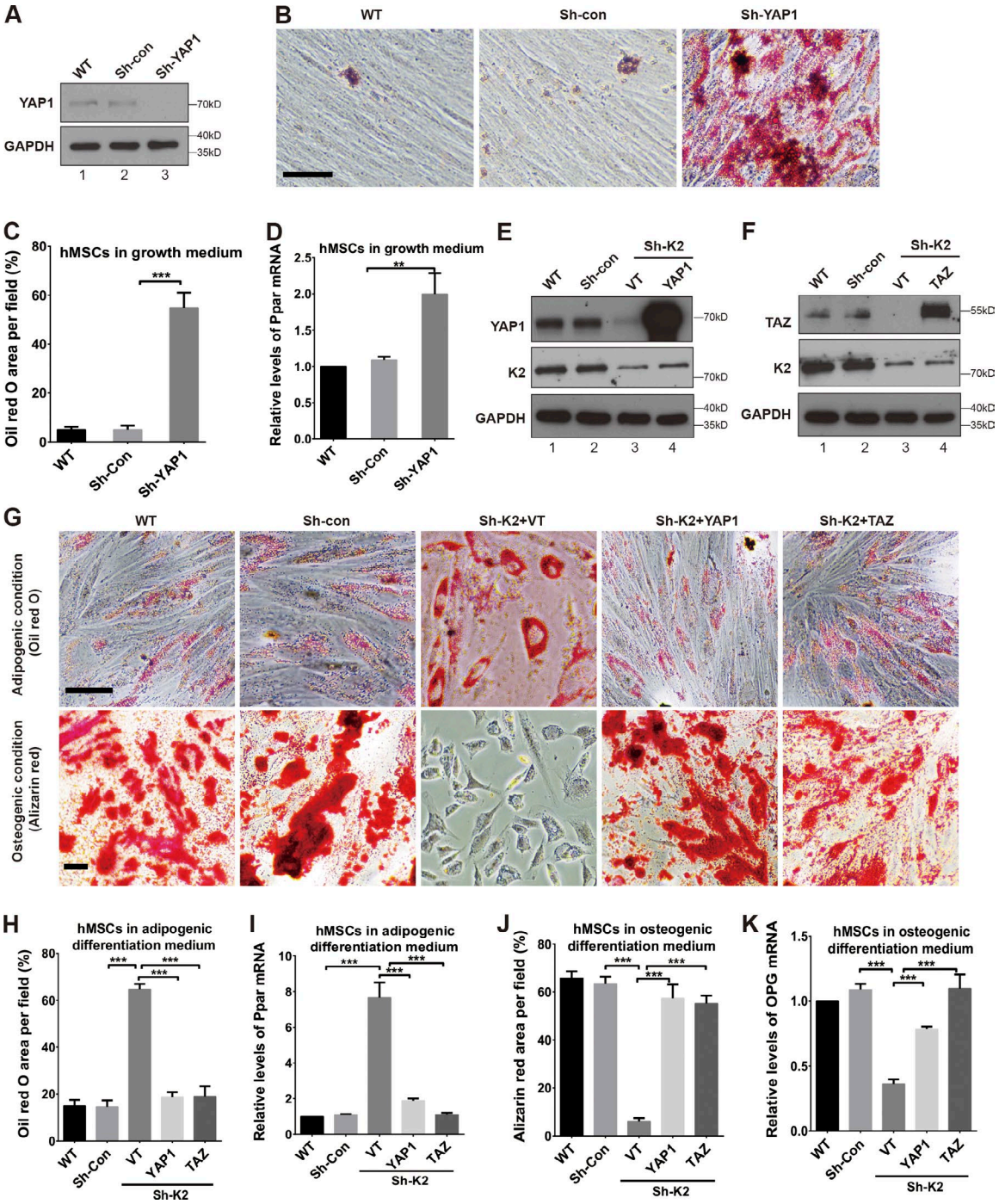

Figure 4. **kindlin-2 regulates MSC differentiation through control of YAP1 and TAZ. (A–D)** Spontaneous adipogenic differentiation of YAP1 knockdown hMSCs. WT hMSCs (lane 1) and hMSCs infected with control (lane 2) or YAP1 shRNA (lane 3) lentivirus were analyzed by Western blotting (A). The cells (as specified in the figure) were cultured in normal culture medium for 14 d and stained with Oil Red O (B). Bar, 50 µm. The percentages of Oil Red area in each macroscopic field (C) were quantified by using ImageJ. Data are means ± SEM; $n = 3$; ***, $P < 0.001$. The mRNA levels of adipogenic markers (Ppar) in the YAP1 knockdown cells were analyzed by RT-PCR and compared with those of the control cells and WT cells (normalized to 1; D). Data are means ± SEM; **, $P < 0.01$; $n = 3$. **(E–K)** hMSCs were infected with kindlin-2 shRNA or control shRNA lentivirus. 2 d after the infection, cells were infected with pLVX lentiviral expression vectors encoding YAP1 or TAZ. 3 d after pLVX-YAP1/TAZ lentiviral infection, the cells were analyzed by Western blotting with antibodies recognizing YAP1, TAZ, kindlin-2, or GAPDH (as a loading control; E and F). The cells treated as above were cultured in adipogenic or osteogenic differentiation medium for 14 d and stained with Oil Red O (top) or Alizarin Red S (bottom) as indicated (G). Bars, 50 µm. The percentages of Oil Red O area (H) and Alizarin Red S area (J) in each macroscopic field were quantified by using ImageJ. Data are means ± SEM; $n = 3$; ***, $P < 0.001$. The levels of mRNAs of adipogenic marker Ppar (I) and osteogenic marker OPG (K) in the cells (as specified in the figure) were analyzed by RT-PCR and compared with those of WT cells (normalized to 1). Data are means ± SEM; ***, $P < 0.001$; $n = 3$.

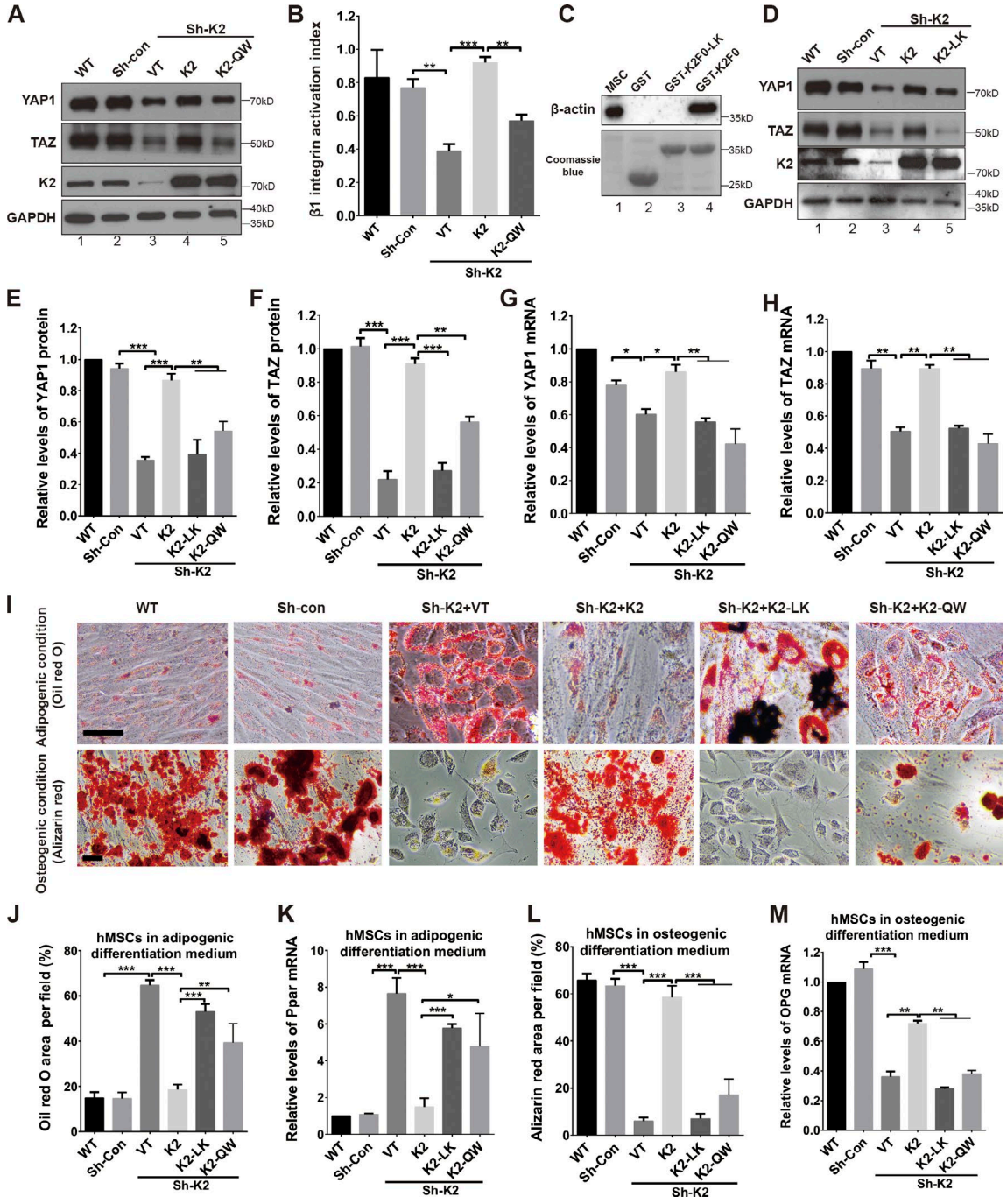

Figure 5. **Integrin- and actin-binding are involved in kindlin-2 regulation of YAP1/TAZ. (A, B, and D–H)** hMSCs were infected with kindlin-2 shRNA (Sh-K2) or control (Sh-con) lentiviruses. 2 d after infection, the cells were infected with lentiviral expression vectors encoding WT kindlin-2 (K2), the actin-binding defective LK/AA mutant (K2-LK), the integrin-binding defective QW/AA mutant (K2-QW), or a control vector lacking kindlin-2 sequence (VT) as described in the Materials and methods. 3 d later, the cells were analyzed by Western blotting (A and D), flow cytometry for integrin activation (B), or RT-PCR (G and H). Western blotting was performed with antibodies recognizing YAP1, TAZ, kindlin-2, or GAPDH (as a loading control) as indicated (A and D). Protein levels of YAP1 (E) and TAZ (F) relative to GAPDH in the infected cells were quantified by densitometry and compared with those in WT cells. Data are means ± SEM; $n = 3$; **, $P < 0.01$; ***, $P < 0.001$. β1 integrin activation was analyzed by flow cytometry as described in the Materials and methods (B). The bars represent means ± SEM; $n = 3$; **, $P < 0.01$; ***, $P < 0.001$. The mRNA levels of YAP1 (G) and TAZ (H) in the control and kindlin-2 knockdown cells or those reexpressing WT or the LK/AA mutant form of kindlin-2 were analyzed by RT-PCR and compared with those in the WT cells (normalized to 1). Data are mean ± SEM; $n = 3$; *, $P < 0.05$; **, $P < 0.01$. **(C)** GST fusion protein pulldown assay was performed by using GST-tagged kindlin-2 F0 fragment (residues 1–105), kindlin-2 F0 fragment (residues 1–105) bearing the LK47/AA mutation, or GST alone as described in the Materials and methods. Actin was detected by Western blotting with an actin antibody (top). The membrane was stained with Coomassie blue (bottom). Lane 1, hMSC lysates. Lanes 2–4, GST or GST fusion protein pulldowns. **(I–M)** The cells (as specified in the figure) were cultured in adipogenic or osteogenic differentiation medium for 14 d and stained with Oil Red O (I, top) or Alizarin Red S (I, bottom). Bars, 50 µm. The percentages of Oil Red O area (J) and Alizarin Red S area (L) per macroscopic field were quantified by using ImageJ. Data are means ± SEM; **, $P < 0.01$; ***, $P < 0.001$; $n = 3$. The levels of mRNAs of adipogenic marker Ppar (K) and osteogenic marker OPG (M) in the control, kindlin-2 knockdown cells, or kindlin-2 knockdown cells reexpressing WT or the LK/AA mutant form of kindlin-2 were analyzed by RT-PCR and compared with those in the WT cells (normalized to 1). Data are means ± SEM; *, $P < 0.05$; **, $P < 0.01$; ***, $P < 0.001$; $n = 3$.

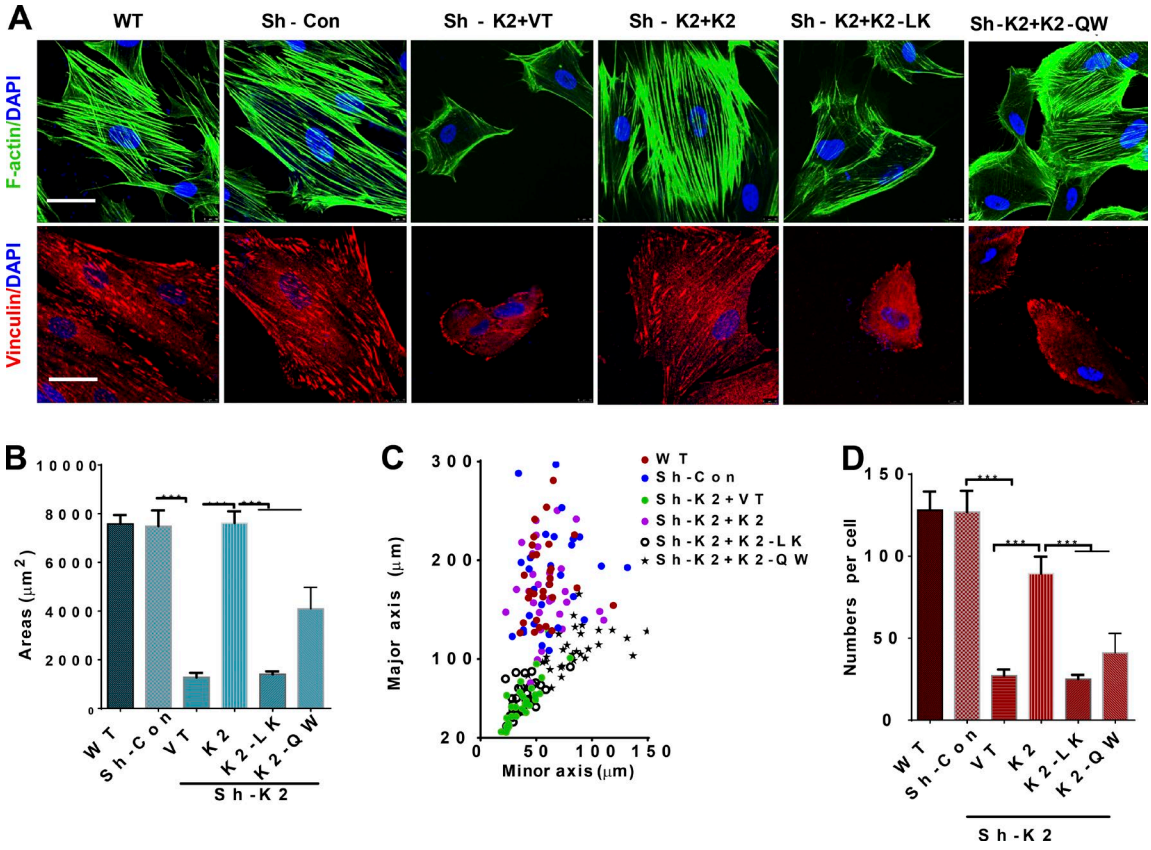

Figure 6. **kindlin-2 regulates MSC geometry, actin stress fiber, and focal adhesion formation.** hMSCs were infected with kindlin-2 shRNA (Sh-K2) or control (Sh-con) lentiviruses. 2 d after infection, the cells were infected with lentiviral expression vectors encoding WT kindlin-2 (K2), the actin-binding defective LK/AA mutant (K2-LK), the integrin-binding defective QW/AA mutant (K2-QW), or a control vector lacking kindlin-2 sequence (VT) as described in the Materials and methods. 3 d later, actin stress fiber organization and focal-adhesion formation were analyzed by immunofluorescent staining of the cells with Alexa Fluor–conjugated phalloidin (topl) and vinculin antibody (bottom), respectively (A). Bars, 50 µm. Cell areas (B), shapes, defined by the lengths of the major and minor axes (C), and focal adhesion number per cell (D) were quantified by using ImageJ. Data are means ± SEM; *n* = 3 experiments; ***, P < 0.001. At least 50 cells were analyzed in each of the groups shown in B and D. The shapes of ∼20 cells from each of the groups were analyzed and presented in C.

of actin stress fiber and focal adhesion (Fig. 6, A–D; and Figs. S5 and S6). Reexpression of kindlin-2, but not that of the LK47/AA mutant, completely reversed the inhibition on the size of hMSCs and formation of actin stress fiber and focal adhesion induced by the knockdown of kindlin-2 (Fig. 6, A–D; and Figs. S5 and S6). Again, consistent with the modest increases of β1 integrin activation and YAP1/TAZ protein levels in response to reexpression of QW615/AA (Fig. 5, A and E–H), reexpression of QW615/AA in kindlin-2–deficient hMSCs modestly increased the size of hMSCs and the formation of actin stress fiber and focal adhesion (Fig. 6, A–D; and Figs. S5 and S6). Nevertheless, the effects of the QW615/AA mutant were significantly weaker than those of WT kindlin-2 (Fig. 6, A–D; and Figs. S5 and S6), indicating that integrin binding is involved in the regulation of these processes.

Kindlin-2 physically associates with MLCK in response to mechanical cues of the MSC microenvironment and promotes myosin light-chain phosphorylation

To investigate the molecular mechanism by which kindlin-2 regulates the actin cytoskeleton, we performed proteomic analyses to identify novel proteins that are associated with kindlin-2. To do this, we immunoprecipitated endogenous kindlin-2 from hMSCs and submitted the anti-kindlin-2 immunoprecipitates for nanoscale liquid chromatography coupled with tandem mass spectrometry (nano LC–MS/MS) analysis. The results showed that MLCK, which is known to phosphorylate myosin light-chain phosphorylation and regulate actomyosin contraction (Goeckeler and Wysolmerski, 1995; Lv et al., 2015), was coimmunoprecipitated with kindlin-2. The association of MLCK with kindlin-2 was confirmed by Western blotting analysis of kindlin-2 immunoprecipitates with anti-MLCK antibodies (Fig. 7 A) and GST-kindlin-2 pulldown assay (Fig. 7 B). Depletion of kindlin-2 significantly reduced the level of MLCK and myosin light-chain phosphorylation (Fig. 7, C–E), suggesting that association with kindlin-2 is important for maintaining the level and activity of MLCK. To further test this, we reexpressed WT, LK47/AA, and QW615/AA mutants of kindlin-2, respectively, in kindlin-2–deficient hMSCs (Fig. 7 F). The results showed that reexpression of WT kindlin-2, but neither LK47/AA nor QW615/AA, reversed the down-regulation of MLCK and myosin light-chain phosphorylation induced by the depletion of kindlin-2 (Fig. 7, F–H), suggesting that integrin- and actin-binding are required for kindlin-2 regulation of MLCK.

We next tested whether the kindlin-2-MLCK association is regulated in response to mechanical cues of cell microenvironment, which are known to be critical for the control of MSC fate

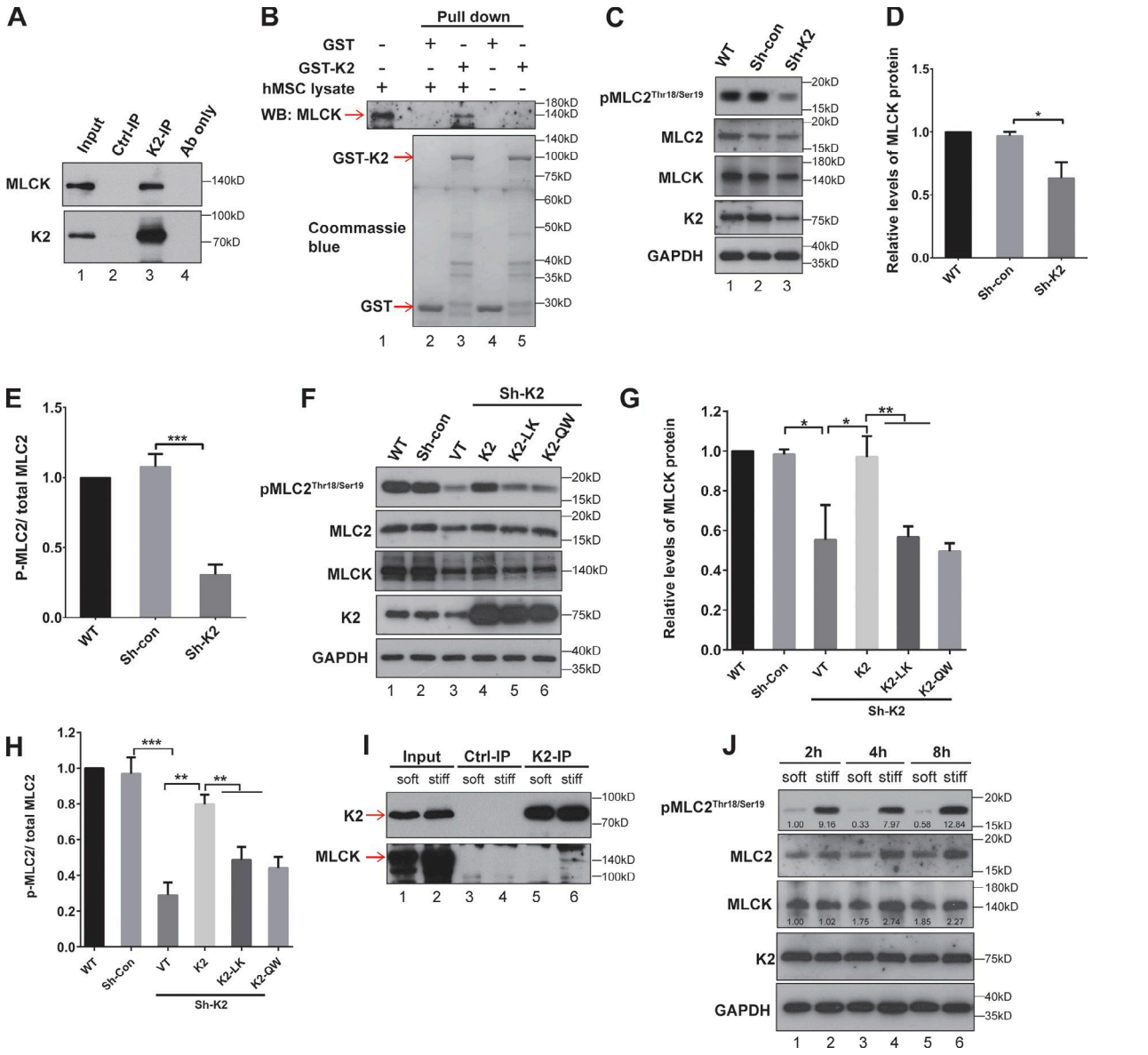

Figure 7. **kindlin-2 associates with MLCK in response to mechanical cues of MSC microenvironment and promotes myosin light chain phosphorylation. (A)** Kindlin-2 forms a complex with MLCK. The lysates of hMSCs cultured under normal conditions were mixed with a kindlin-2 antibody or control IgG. The cell lysates (lane 1), control IgG immunoprecipitates (lane 2), kindlin-2 antibody immunoprecipitates (lane 3), or kindlin-2 antibody alone (lane 4) were analyzed by Western blotting with kindlin-2 or MLCK antibody. **(B)** GST-fusion protein pulldown assay was performed by using GST-tagged kindlin-2 or GST as a control. MLCK was detected by Western blotting with actin antibody (top). The membrane was stained with Coomassie blue (bottom). Lane 1, hMSC lysates. Lanes 2–5, GST or GST-fusion protein pulldowns. **(C–E)** hMSCs were infected with kindlin-2 shRNA or control lentivirus, cultured in normal medium for 5 d and analyzed by Western blotting with antibodies recognizing pMLC2Thr$^{18/Ser19}$, MLC2, MLCK, kindlin-2, or GAPDH (as a loading control; C). The levels of MLCK (relative to GAPDH; D) and pMLC2Thr$^{18/Ser19}$ (relative to total MLC2; E) in the infected hMSCs were quantified by densitometry and compared with those in the WT hMSCs (normalized to 1). The bars represent means ± SEM; $n = 3$; *, $P < 0.05$; ***, $P < 0.001$. **(F–H)** hMSCs were infected with kindlin-2 shRNA (Sh-K2) or control (Sh-con) lentiviruses. 2 d after infection, the cells were infected with lentiviral expression vectors encoding WT kindlin-2 (K2), the actin-binding defective LK/AA mutant (K2-LK), the integrin-binding defective QW/AA mutant (K2-QW), or a control vector lacking kindlin-2 sequence (VT) as described in the Materials and methods. 3 d after the lentiviral infection, the cells were analyzed by Western blotting with antibodies recognizing pMLC2$^{Thr18/Ser19}$, MLC2, MLCK, kindlin-2, or GAPDH (as a loading control; F). The levels of MLCK (relative to GAPDH; G) and pMLC2Thr$^{18/Ser19}$ (relative to total MLC2; H) in the infected hMSCs were quantified by densitometry and compared with those in the WT hMSCs (normalized to 1). The bars represent means ± SEM; $n = 3$; *, $P < 0.05$; **, $P < 0.01$; ***, $P < 0.001$. **(I)** hMSCs were plated on stiff or soft hydrogels for 4 h. The complex formation between kindlin-2 and MLCK was analyzed by coimmunoprecipitation as described in A. **(J)** hMSCs were plated on stiff or soft hydrogels for 2 h, 4 h, and 8 h and then analyzed by Western blotting with antibodies recognizing pMLC2Thr$^{18/Ser19}$, MLC2, MLCK, kindlin-2, or GAPDH (as a loading control). The intensities of the protein bands were quantified by densitometry. The numbers indicate the levels of MLCK (relative to GAPDH) and pMLC2Thr$^{18/Ser19}$ (relative to total MLC2). The experiments were repeated twice, and similar results were obtained.

determination (Connelly et al., 2010; Dupont et al., 2011; Halder et al., 2012; Hao et al., 2014; Lv et al., 2015). To do this, we plated hMSCs on soft and stiff matrices and analyzed the effects on the association of MLCK with kindlin-2 by coimmunoprecipitation. The results showed that, although MLCK was coimmunoprecipitated with kindlin-2 in hMSCs plated on stiff matrices (Fig. 7 I, lane

6), no MLCK was detected in the kindlin-2 immunoprecipitates derived from hMSCs plated on soft matrices (Fig. 7 I, lane 5). Thus, the kindlin-2-MLCK association is influenced by mechanical cues of cell microenvironment (i.e., substrate stiffness). Consistent with a role of kindlin-2 in regulation of MLCK activity, the level of myosin light-chain phosphorylation was also markedly reduced in hMSCs on soft matrices compared with that in hMSCs on stiff matrices (Fig. 7 J, compare lanes 1, 3, and 5 with lanes 2, 4, and 6).

Kindlin-2 regulates RhoA activation

Previous studies have shown that RhoA is involved in mechanoregulation of YAP1/TAZ (McBeath et al., 2004; Jaalouk and Lammerding, 2009; Mammoto and Ingber, 2009; Wozniak and Chen, 2009; Halder et al., 2012). Consistent with previous studies and similar to the effect of depletion of kindlin-2 (Fig. 3, A–D), treatment of hMSCs with RhoA inhibitor C3 transferase reduced the levels of YAP1/TAZ proteins (Fig. 8, A–C). However, unlike depletion of kindlin-2 (Fig. 3, E and F), treatment with RhoA inhibitor C3 transferase did not reduce the levels of YAP1/TAZ mRNAs (Fig. 8, D and E).

We next tested the effect of depletion of kindlin-2 on RhoA activation using a modified fluorescence resonance energy transfer (FRET)–based RhoA biosensor (Aoki and Matsuda, 2009). The results showed that depletion of kindlin-2 significantly inhibited the activation of RhoA (Fig. 8, F–H). This was confirmed by measuring RhoA activation by using a G-LISA assay (Fig. 8 I). The inhibition of RhoA was significantly reversed by reexpression of WT but not that of the LK47/AA or QW615/AA mutant forms of kindlin-2 (Fig. 8 I). Interestingly, inhibition of RhoA with C3 transferase significantly reduced the association of MLCK with kindlin-2 (Fig. 8 J) and concomitantly inhibited myosin light-chain phosphorylation (Fig. 8, K and L).

Kindlin-2 regulates YAP1 through an AIP4-dependent but LATS1-independent mechanism

YAP1/TAZ can be regulated by multiple signaling pathways including large tumor suppressor kinase 1 (LATS1)– or AIP4-dependent and -independent pathways (Hao et al., 2008; Oka et al., 2008; Zhang et al., 2008; Zhao et al., 2010; Chen et al., 2016). We first tested whether kindlin-2–mediated regulation of YAP1/TAZ depends on LATS1. Because LATS1 can catalyze YAP1 phosphorylation at Ser127 (Gregorieff et al., 2015; Moroishi et al., 2015; Chen et al., 2016; Hong et al., 2016), which is known to promote cytoplasmic localization and degradation of YAP1 (Zhao et al., 2010), we tested the effect of kindlin-2 knockdown on phosphorylation of YAP1 at Ser127. As expected, knockdown of kindlin-2 reduced the total level of YAP1 protein (Fig. 9 A). However, the ratio of Ser127-phosphor-YAP1/YAP1 was higher in kindlin-2–deficient hMSCs compared with that in control hMSCs (Fig. 9, A and B), albeit the absolute level of Ser127-phosphor-YAP1 was reduced in kindlin-2 deficient hMSCs compared with that in control hMSCs (Fig. 9 A, compare lane 3 with lanes 1 and 2). Thus, depletion of kindlin-2 reduces the protein level of YAP1 but increases the efficiency of YAP1 phosphorylation at Ser127. Consistent with this, the nuclear localization of YAP1 was significantly reduced in response to knockdown of kindlin-2 (Fig. 9, C and D). Interestingly, in contrast to the increase of the efficiency of YAP1 phosphorylation at Ser127 in response to kindlin-2 deficiency, depletion of kindlin-2 reduced rather than increased the level of LATS1 (Fig. 9 A, compare lane 3 with lanes 1 and 2), suggesting that the increased efficiency of YAP1 phosphorylation at Ser127 induced by the depletion of kindlin-2 was not caused by the increase of the level of LAST1. To further investigate the role of LATS1 in kindlin-2 regulation of YAP1 phosphorylation at Ser127, we knocked down both LATS1 and kindlin-2, or LATS1 alone as a control, and assessed the effect on YAP1 phosphorylation at Ser127. The results showed that, whereas knockdown of LATS1 significantly reduced YAP1 phosphorylation at Ser127 in control MSCs that express a normal level of kindlin-2 (Fig. 9, A and B), knockdown of LATS1 did not significantly reduce the level of Ser127 phosphorylation of YAP1 in kindlin-2–deficient cells (Fig. 9, A and B). Consistent with this, depletion of LATS1 did not reverse the nuclear exclusion of YAP1 induced by kindlin-2 knockdown (Fig. 9, C and D). Collectively, these results suggest that the increase of Ser127-phosphorylation and nuclear exclusion of YAP1 in response to loss of kindlin-2 does not depend on LATS1.

We next tested whether AIP4 is involved in kindlin-2 regulation of YAP1/TAZ. To do this, we depleted AIP4 from kindlin-2 knockdown hMSCs and assessed the effects on YAP1/TAZ. The results showed that depletion of AIP4 markedly reversed the down-regulation of YAP1/TAZ induced by the knockdown of kindlin-2 (Fig. 10, A–C). Furthermore, it restored to a large extent nuclear localization of YAP1/TAZ (Fig. 10, D and E). Thus, AIP4 is required for kindlin-2–mediated regulation of the protein levels and nuclear localization of YAP1/TAZ.

Discussion

MSCs are common progenitor cells for different cell lineages including adipocytes and osteoblasts (Bianco et al., 2001; Wu et al., 2010; Chen et al., 2016). The decision for MSC commitment to a particular cell lineage is precisely controlled during tissue and organ development and regeneration, and dysregulation of this process is frequently found in human diseases (Wu et al., 2010). The molecular mechanism that controls the commitment of MSCs to differentiate into different cell lineages is complex and incompletely understood (Sordella et al., 2003). In this study, we have identified kindlin-2 as a key determinant of MSC commitment to different cell lineages and delineated the underlying signaling mechanism.

Several lines of evidence suggest that kindlin-2 plays a critical role in control of cell lineage commitment of MSCs. First, the level of kindlin-2 is markedly changed during MSC differentiation in vitro and in vivo: It is significantly increased during osteogenic differentiation but reduced during adipogenic differentiation. Second, forced reduction of the level of kindlin-2 in MSCs is sufficient to induce spontaneous adipogenesis and inhibit osteogenesis, even when MSCs are stimulated with soluble factors that would normally induce osteogenesis. Third, using both conditional kindlin-2 knockout mouse model and MSC transplantation model, we show that depletion of kindlin-2 promotes adipogenesis and inhibits osteogenesis in mice, confirming an antiadipogenesis and pro-osteogenesis role of kindlin-2 in vivo.

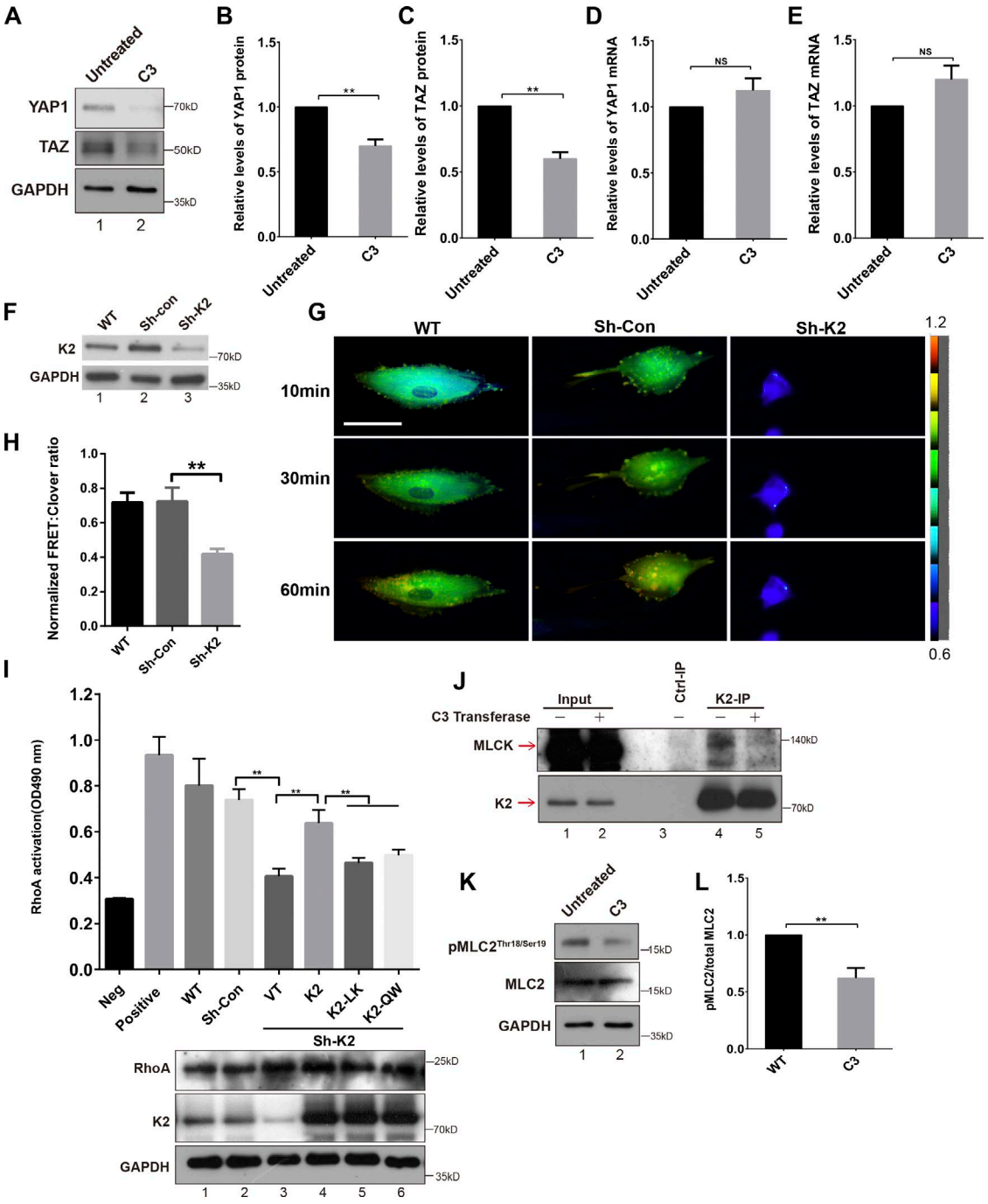

Figure 8. **kindlin-2 regulates RhoA activation. (A–E)** hMSCs were treated with (lane 2) or without (lane 1) Rho inhibitor C3 (3 µg/ml) for 24 h and analyzed by Western blotting with antibodies recognizing YAP1, TAZ, or GAPDH (as a loading control; A). The protein levels of YAP1 (B) and TAZ (C) relative to GAPDH in the C3-treated cells were quantified by densitometry and compared with those in the untreated cells (normalized to 1). The bars represent means ± SEM; $n = 3$; **, $P < 0.01$. The mRNA levels of YAP1 (D) and TAZ (E) in hMSCs treated with C3 were analyzed by RT-PCR and compared with those in the untreated cells (normalized to 1). The bars represent means ± SEM; $n = 3$. **(F–H)** hMSCs were infected with kindlin-2 shRNA lentivirus or control lentivirus. 2 d after the infection, some of the cells were analyzed by Western blotting to confirm knockdown of kindlin-2 (F). The remaining cells were infected with adenovirus encoding Clover-RhoA-RKN-Rubby. 3 d later, cells were replated onto fibronectin-coated dishes for 24 h, and RhoA activation was then analyzed by FRET with time-lapse microscopy (images were acquired for 60 min at 1-min intervals) as described in the Materials and methods. Representative FRET/Clover ratio images at the indicated time points (10, 30, and 60 min) are shown (G). Bar, 50 µm. Normalized FRET/Clover ratio of the kindlin-2 knockdown cells at 60 min was compared with that of the control infectants and WT (WT) hMSCs at the same time point. Data are means ± SEM; $n = 5$; **, $P < 0.01$(H). **(I)** hMSCs were infected with kindlin-2 shRNA (Sh-K2) or control (Sh-con) lentiviruses. 2 d after infection, the cells were infected with lentiviral expression vectors encoding WT kindlin-2 (K2), the actin-binding defective LK/AA mutant (K2-LK), the integrin-binding defective QW/AA mutant (K2-QW), or a control vector lacking kindlin-2 sequence (VT) as described in the Materials and methods. 3 d after the lentiviral infection, RhoA activation was measured by G-LISA. Data are mean ± SEM; $n = 3$; *, $P < 0.05$; **, $P < 0.01$; ***, $P < 0.001$ (top). Negative control (Neg), buffer blank control; positive control; RhoA-positive control were provided by the kit. Total RhoA, kindlin-2, and GAPDH (as a loading control) were analyzed by Western blot (bottom). **(J)** The complex formation between kindlin-2 and MLKC in C3-treated and untreated cells was analyzed by coimmunoprecipitation and Western

How does kindlin-2 control the cell fate decision of MSCs? The studies described in this paper suggest that kindlin-2 controls this process primarily through regulation of YAP1/TAZ. First, the levels of YAP1/TAZ are closely correlated with that of kindlin-2 during adipogenic differentiation and osteogenic differentiation, both in cultured MSCs and in vivo. Second, depletion of kindlin-2 markedly reduces the levels of YAP1/TAZ in culture and in vivo, whereas overexpression of kindlin-2 promotes YAP1/TAZ expression, indicating that kindlin-2 acts upstream of YAP1/TAZ and controls their levels. Third and perhaps most importantly, forced up-regulation of YAP1 or TAZ expression is able to restore to a large extent the ability of MSCs to differentiate into osteocytes and reverse the spontaneous adipogenic differentiation induced by the loss of kindlin-2.

How does kindlin-2 regulate YAP1/TAZ? The studies presented in this paper suggest that kindlin-2 regulates YAP1 and TAZ through two distinct mechanisms, one controlling YAP1/TAZ proteins and the other controlling YAP1/TAZ transcripts. Using a combination of proteomic, cell biological, and genetic approaches, we have obtained important information on the mechanism by which kindlin-2 regulates YAP1/TAZ proteins and consequently MSC fate decision. Based on the findings obtained from this and other studies, we propose a model in which kindlin-2 serves as a key component of the signaling pathway that senses the mechanical environment and controls YAP1/TAZ expression, degradation, and nuclear localization and ultimately MSC differentiation. Specifically, kindlin-2 physically associates with MLCK (Fig. 7, A and B), which is regulated by mechanical cues of MSC microenvironment (e.g., stiffness of matrices; Fig. 7 I) and intracellular signaling events (e.g., RhoA activation; Fig. 8 H), and regulates myosin light-chain phosphorylation (Fig. 7, C–F) and consequently actin cytoskeleton organization, YAP1/TAZ phosphorylation, degradation, and nuclear localization, and thereby controls YAP1/TAZ-mediated gene expression and MSC differentiation. Interestingly, although RhoA regulates kindlin-2 association with MLCK and myosin light-chain phosphorylation, the activation of RhoA itself is also regulated by kindlin-2, because depletion of kindlin-2 diminishes RhoA activation (Fig. 8, F and G). Thus, there is a positive regulatory cycle between RhoA and kindlin-2 (removing either one will inhibit the other), leading to augmented actin stress fiber formation and contraction and consequently increased levels and nuclear localization of YAP1/TAZ that controls MSC differentiation. It appears that AIP4 serves as a key downstream effector of kindlin-2 in this signaling pathway, because depletion of AIP4 significantly reverses the down-regulation of YAP1/TAZ levels induced by the depletion of kindlin-2 (Fig. 10). In contrast, depletion of LATS1 did not significantly reduce the Ser127 phosphorylation and nuclear exclusion of YAP1 induced by the depletion of kindlin-2 (Fig. 9), suggesting that LATS1 is not essential for kindlin-2 regulation of YAP1. It is important to note that the reversal induced by the depletion of AIP4 is incomplete (the levels of YAP1/TAZ remain ∼20–30% lower in kindlin-2 and AIP4 double-knockdown cells compared with those in control cells; Fig. 10, B and C), suggesting that there exists a second mechanism through which kindlin-2 regulates YAP1/TAZ. In this regard, it is worth noting that kindlin-2 regulates YAP1/TAZ at not only the protein but also the mRNA levels (Fig. 3). Both the actin- and integrin-binding are involved in the kindlin-2–mediated regulation of YAP1/TAZ mRNAs (Fig. 5, E and F). However, because inhibition of RhoA, unlike depletion of kindlin-2, does not reduce the YAP1/TAZ mRNA levels (Fig. 8, D and E), the regulation of YAP1/TAZ mRNAs is independent of RhoA. Interestingly, although abundant kindlin-2 is detected at cell–matrix adhesions (Fig. S4; Tu et al., 2003), our preliminary studies suggest that a fraction of kindlin-2 can localize to the nuclei of MSCs under certain conditions (e.g., in MSCs plated on a micropatterned fibronectin-coated surface with a diameter of 50 µm; Fig. S6). Whether nuclear kindlin-2 is directly involved in the transcriptional regulation of YAP1/TAZ will be an important area of future studies.

In summary, our studies have identified kindlin-2 as a key determinant of MSC lineage commitment and delineated a novel signaling pathway consisting of kindlin-2, RhoA, MLCK, AIP4, and YAP1/TAZ that senses the mechanical cues of the cell microenvironment and controls MSC fate decision. The findings described in this paper provide mechanistic insight as to why loss of kindlin-2 is detrimental to MSC differentiation and skeletal development. Given the importance of MSC differentiation in tissue repair and regeneration, our findings may help develop novel therapeutic approaches to control these processes.

Materials and methods

Mice

PRX1-Cre transgenic mice and kindlin-2$^{fl/fl}$ mice were generated as we described (Wu et al., 2015). Nu/Nu mice were bought from Vital River Laboratory Animal Technology Co. Ltd. All mouse work was performed with the approval of the Institutional Animal Care and Use Committee, Southern University of Science and Technology.

DNA constructs, lentivirus production, and infection

The pLKO.1, psPAX2, and pMD2.G vectors were from Addgene (plasmid 10878). The pLKO.1 vectors expressing shRNAs targeting human kindlin-2, LATS1, GFP, or scrambled shRNA (sh-con) sequence were generated by using the following sequences: Sh-Kindlin-2: 5′-AACAGCGAGAATCTTGGAGGC-3′; Sh-LATS1: 5′-GAGAAATTAAGCCATCGTGTT-3′; Sh-GFP: 5′-GCAAGCTGACCCTGAAGTTCA-3′; Sh-con: 5′-ACGCATGCATGCTTGCTTT-3′. To generate lentiviruses encoding these shRNAs, 293T cells were

blot with kindlin-2 and MLCK antibodies. Lanes 1 and 2, cell lysates. Lane 3, control IgG immunoprecipitates. Lanes 4 and 5, kindlin-2 immunoprecipitates. **(K and L)** hMSCs were treated with Rho inhibitor C3 (3 µg/ml) for 24 h and analyzed by Western blotting with antibodies recognizing pMLC2$^{Thr18/Ser19}$, MLC2, or GAPDH (as a loading control; K). Protein levels of pMLC2$^{Thr18/Ser19}$ relative to total MLC2 in the C3-treated cells were quantified by densitometry and compared with untreated cells (normalized to 1). The bars represent means ± SEM; $n = 3$; **, $P < 0.01$ (L).

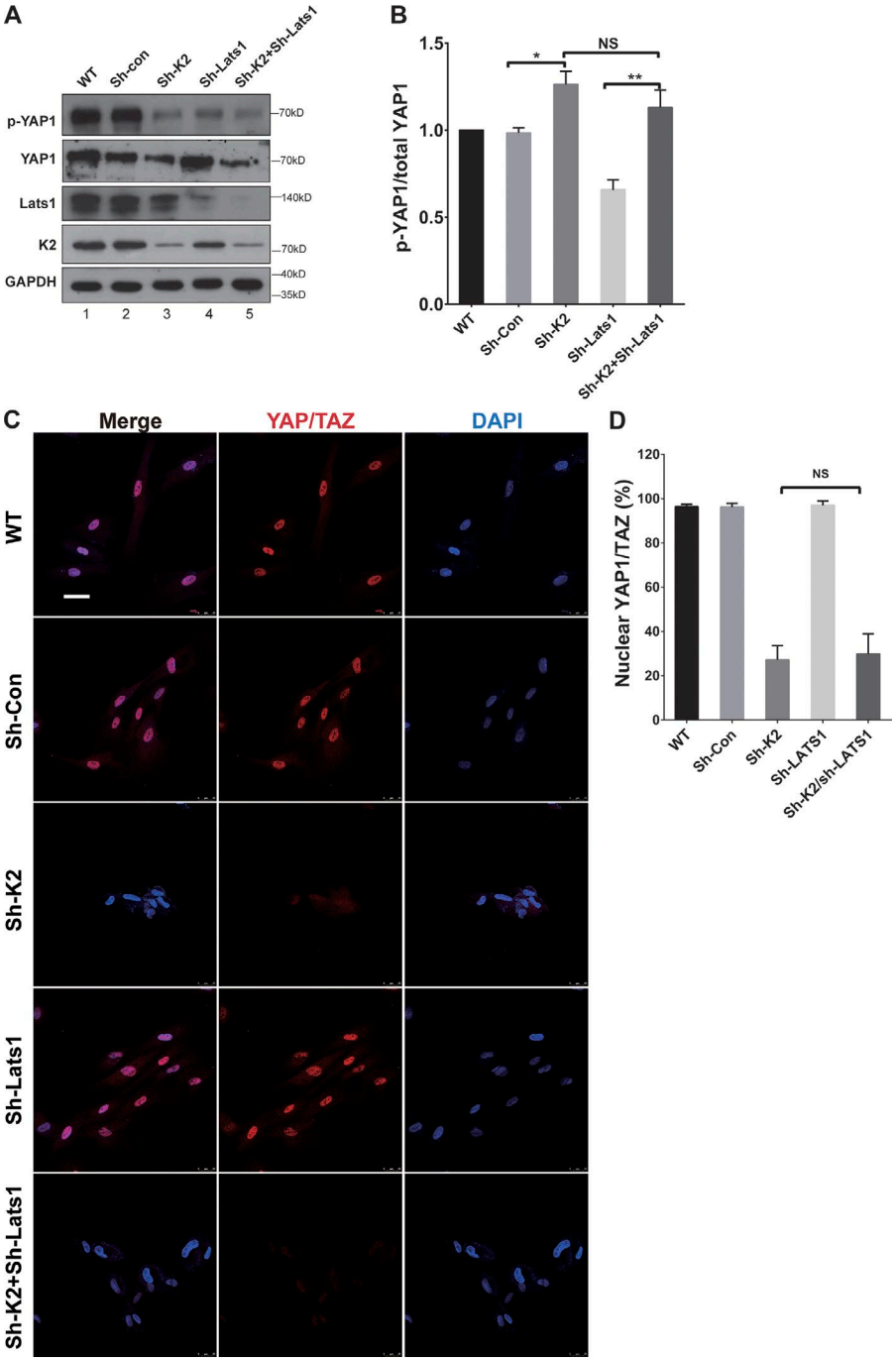

Figure 9. **kindlin-2 regulates YAP/TAZ in a Lats1-independent manner.** hMSCs were infected with kindlin-2 shRNA lentivirus (sh-K2), Lats1 shRNA lentivirus (sh-Lats1), control lentivirus (sh-Con), or both sh-kindlin-2 and sh-Lats1 (sh-K2+ sh-Lats1). The cells were cultured in normal medium for 5 d and analyzed by Western blotting (A) with antibodies recognizing YAP1, p-YAP1(Ser127), or GAPDH (as a loading control). The ratios of the level of Ser127-phosphorylated YAP1 versus total YAP1 (p-YAP1(Ser127)/YAP1) in infected hMSCs were quantified by densitometry and compared with those in the WT (WT) hMSCs (normalized to 1; B). The bars represent means ± SEM; $n = 3$; *, $P < 0.05$; **, $P < 0.01$. The cells were analyzed by immunofluorescent staining with DAPI and YAP1/TAZ antibodies (C). Bar, 50 µm. The percentages of cells with nuclear YAP1/TAZ were quantified (D). At least 100 cells were counted in each experiment. Bars represent means ± SEM; $n = 3$.

cotransfected with pLKO.1 encoding the various shRNAs, psPAX2 and pMD2. G. The pLVX vector was a gift from J. Weber (Washington University, St. Louis, MO) and Z. Yandong (Southern University of Science and Technology, Shenzhen, China). The expression vectors (pLVX-YAP1, pLVX-TAZ, pLVX-kindlin-2 WT [K2-WT], pLVX-K2-LK, and pLVX-K2-QW) encoding human YAP1 or TAZ and WT or mutant forms of kindlin-2 (LK47/AA mutant [Bledzka et al., 2016] or QW/AA mutant [Shi et al., 2007; Ma et al., 2008]) were generated by cloning the corresponding cDNA sequences into the pLVX vector. The sequence corresponding to the shRNA targeting region in the kindlin-2 expression vectors was changed to 5′-AACCGCCAGGATTTTGGAGGC-3′ to confer resistance to the kindlin-2 shRNA. The sequences of all DNA inserts were verified by DNA sequencing (Invitrogen). To generate lentiviral expression vectors encoding YAP1, TAZ, K2-WT, or mutant forms of kindlin-2 (K2-QW or K2-LK), pLVX-YAP1, pLVX-TAZ, pLVX-K2-WT, pLVX-K2-QW, or pLVX-K2-LK were cotransfected with psPAX2 and pMD2.G into 293T cells. For lentiviral or adenovirus infection, hMSCs were cultured in basal growth medium until 70% confluence and then replaced with fresh medium containing lentivirus or adenovirus at an MOI of 100 for 16 h. Lentiviral infections were performed in the presence of 8 µg/ml polybrene. Adenovirus-Cre, adenovirus-laz, and adenovirus expressing Clover-RhoA-RKN-Rubby were from Biochuan company.

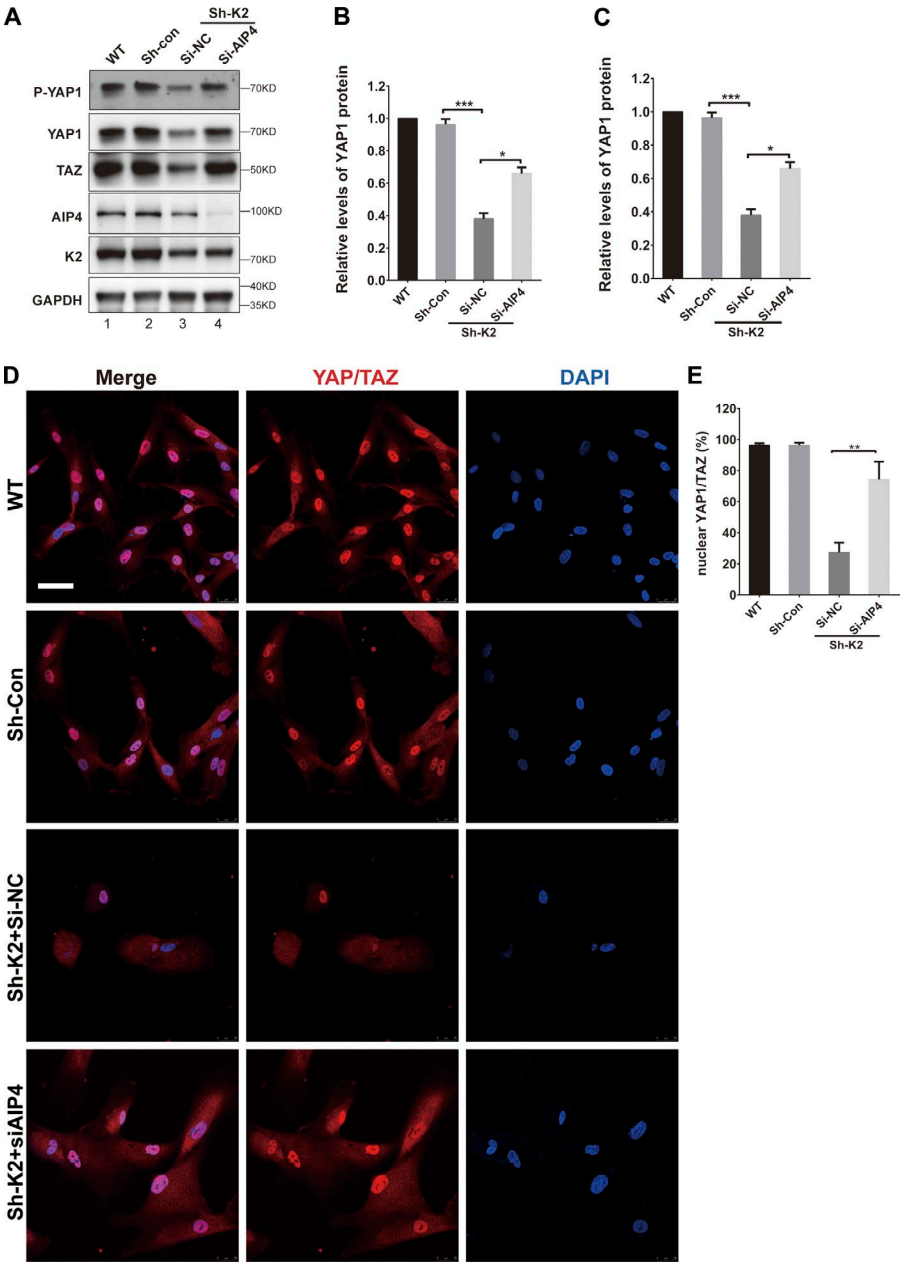

Figure 10. **AIP4 mediates kindlin-2 regulation of YAP1/TAZ proteins. (A–E)** hMSCs were infected with kindlin-2 shRNA or control shRNA lentivirus. 2 d later, the cells were transfected with siRNA targeting AIP4 (siAIP4) or a control siRNA (siNC). 3 d after transfection, the cells were analyzed by Western blotting with antibodies recognizing p-YAP1, YAP1, TAZ, kindlin-2, AIP4, or GAPDH (as a loading control; A). Protein levels of YAP1 (B) and TAZ (C) relative to that of GAPDH in the infected cells were quantified by densitometry and compared with that of WT hMSCs (normalized to 1) by using ImageJ. The bars represent means ± SEM; $n = 3$; *, $P < 0.05$; ***, $P < 0.001$. The cells were immunofluorescently stained with DAPI and YAP1/TAZ antibody (D). Bar, 50 µm. The percentages of nuclear YAP/TAZ positive cells among total cells were quantified (E). Data are means ± SEM; $n = 3$; **, $P < 0.01$. At least 100 cells were counted in each experiment.

Cell isolation and culture

hMSCs were isolated from human placenta as previously described (Guo et al., 2014; Wang et al., 2015). In brief, term (38- to 40-wk-gestation) placentas from healthy donors were harvested with written informed consent, and the procedure was approved by the Ethics Committee of Meilin Hospital. The placental tissue was washed several times with cold PBS and then mechanically minced and enzymatically digested with 0.25% trypsin-EDTA for 30 min at 37°C in a water bath. The digest was subsequently filtered, pelleted, and resuspended in a growth medium consisting of DMEM (Gibco-Invitrogen), 10% FBS (Gibco-Invitrogen), and antibiotics. Cells were seeded on cell culture dishes, and medium was replaced every 2 d to reach 80% confluence. For RhoA inhibition studies, cells were cultured in DMEM containing 3 µg/ml cell-permeable C3 transferase (Cytoskeleton Inc.) for 24 h and then harvested and analyzed as specified in each experiment.

Differentiation of hMSCs in culture

hMSCs were seeded in 12-well tissue culture plates (Corning) and cultured in various media as specified in each experiment. For induction of adipogenic differentiation, hMSCs were cultured in DMEM supplemented with 10% FBS, 1% penicillin-streptomycin, 125 µM 3-isobutyl-1-methylxanthine (Sigma-Aldrich), 0.25 µM dexamethasone (Sigma-Aldrich), 2.5 µM insulin (Sigma-Aldrich), and 50 µM indomethacin (Sigma-Aldrich). 14 d later, cells were fixed in 4% paraformaldehyde and stained with Oil Red O (Sigma-Aldrich) until obvious signals were detected in one or more of the cell groups (e.g., sh-K2 cell group; Wu et al., 2007; Li et al., 2011; Guo et al., 2014). The cells were then rinsed three times with PBS to stop the staining. For induction of osteogenic differentiation, hMSCs were cultured in DMEM-high glucose supplemented with 10% FBS, 1% penicillin-streptomycin, 10 nM dexamethasone, 50 µM ascorbic acid 2-phosphate

(Sigma-Aldrich), and 10 mM β-glycerophosphate (Sigma-Aldrich). 14 d later, cells were fixed in 4% paraformaldehyde and stained with Alizarin Red S (Sigma-Aldrich) to observe mineralized matrix deposition (Wu et al., 2007; Li et al., 2011; Guo et al., 2014). Images were acquired at room temperature by using a microscope (Eclipse TS100; Nikon) with LWD 10×/0.25 and LWD 20×/0.4 objectives (Nikon) equipped with a digital camera (TS100-F; Nikon) and NIS-Elements F Ver 4.00.00 (Nikon) image software. The data were analyzed with ImageJ software. Oil Red O or Alizarin Red S staining areas per macroscopic field were analyzed by using ImageJ. The numbers from five microscopic fields (from the center and four sides of the well at 20× magnification) were quantified, and the means ± SEM were calculated using one-way ANOVA.

RNA interference

siRNA directed against human AIP4 was synthesized by Invitrogen. The sense sequence of siRNA for human AIP4 was 5′-GCC TATGTTCGGGACTTCAAA-3′ and that of the control siRNA was 5′-ACGCATGCATGCTTGCTTT-3′. Transfection of siRNAs to hMSCs was performed by using Lipofectamine RNAiMAX Reagent (Life Technologies). Cells were transfected with 25 pmol per six-well culture dish (1×10^5 cells/ml in six-well plates).

Quantitative RT-PCR analysis

Total RNA was extracted from hMSCs or newborn femur tissue with TRIzol (Invitrogen) by following the manufacturer's instructions. First-strand cDNA was prepared by reverse transcription with Superscript II reverse transcription (Invitrogen) and oligo(dT) primers and stored at 20°C. RT-PCR was performed by using SYBR Premix Ex Taq II on an ABI 7500 QPCR System. As an internal control, levels of GAPDH mRNA were quantified in parallel with mRNAs of the target genes. Normalization and fold changes were calculated by using the ΔΔCt method. Primer sets are listed in Table S1.

Protein extraction from bone

Proteins from femurs were extracted by using a previously described protocol (Jiang et al., 2007; Wu et al., 2015). Briefly, femur bone tissues of the newborn mice were carefully defleshed, and bone marrow was flushed out. Femurs were homogenized and incubated on ice for 30 min in 1× lysis buffer (50 mM Tris-HCl, pH 7.4, 250 mM NaCl, 2 mM EDTA, 2 µg/ml aprotinin, 1 mM DTT, 1 mM PMSF, 1 mM NaF, 0.5 µg/ml leupeptin, and 1% SDS). The lysate was centrifuged at 10,000 rpm at 4°C for 30 min. Protein concentration was determined by using a BCA assay (Thermo Fisher Scientific).

Western blotting

Western blotting was performed as previously described (Wu et al., 2015). For the preparation of whole-cell protein lysates, cells were lysed in RIPA (20 mM Tris-HCl [pH 7.5], 150 mM NaCl, 1 mM Na_2 EDTA, 1% Nonidet P-40, 1% sodium deoxycholate). Equal amounts (40–60 µg per lane) of total protein were separated on 10% polyacrylamide gel and transferred onto a nitrocellulose membrane. Membranes were blocked for 1 h at room temperature in Tris-buffered saline (50 mM Tris-HCl and 150 mM NaCl, pH 7.4) containing 0.1% Tween 20 and 5% nonfat powdered milk, followed by overnight incubation at 4°C with mouse anti-GAPDH (M20006; Abmart), rabbit anti–kindlin-1 (ABT422, Millipore), rabbit anti–kindlin-3 (10459S; Cell Signaling), mouse anti–kindlin-2 (clone 3A3.5; Tu et al., 2003; Wu et al., 2015), mouse anti–β-actin (ab8226; Abcam), rabbit anti-LATS1 (3477S; Cell Signaling), mouse anti-YAP1/TAZ (sc-101199; Santa Cruz), mouse anti-MLCK (M7905; Sigma-Aldrich), rabbit anti–p-MLC2$^{Thr18/Ser19}$ (3674; Cell Signaling), rabbit anti-MLC2 (3672; Cell Signaling), rabbit anti–p-YAP1(4911S; Cell Signaling), mouse anti-RhoA (sc-418; Santa Cruz), rabbit anti-ALP (GTX62596; Genetex), or rabbit anti-AIP4 (12117S; Cell Signaling) antibodies. After washing and incubation with appropriate HRP-conjugated secondary anti–rabbit or –mouse IgG antibodies (711-005-152 or 715-005-151; Jackson ImmunoResearch), blots were developed by using an ECL kit (Bio-Rad) and then exposed to x-ray film (super RX-N-C; Fuji Film). The images were scanned by using an imaging scanning system (L365; EPSON Scan). Quantification of the densitometry was performed by using ImageJ.

Immunofluorescence

hMSCs (2×10^4 per well) were seeded on coverslips in 24-well plates and cultured overnight. The cells were then immersed in 0.1% Triton X-100 in PBS for 10 min at room temperature, followed by washing three times with PBS. The cells were incubated with mouse anti-YAP1/TAZ (sc-101199; Santa Cruz), mouse anti–kindlin-2 (clone 3A3.5), rabbit anti-Ki67 antibody (ab16667; Abcam), rabbit anti-ALP (GTX62596; Genetex), rabbit anti-perilipin (9391S; Cell Signaling), and mouse anti-vinculin antibodies (ab18058; Abcam) at 4°C overnight. The cells were then washed with PBS and incubated with Alexa Fluor 594/488–conjugated anti–mouse or –rabbit (Invitrogen) secondary antibodies (1:300) for 1 h at room temperature. In some experiments, the cells were costained with Alexa Fluor–phalloidin (Life Technologies) and/or DAPI for 30 min at room temperature. Images were acquired at 21°C using an SP8 confocal fluorescence microscope (20× dry objective 0.7 NA, 40× dry objective 0.85 NA, or 63× oil objective 1.4 NA; Leica) with Leica X Version 1.1.0.12420 image software. The numbers of Ki67$^+$, ALP$^+$, and Perilipin$^+$ cells were quantified from five microscopic fields (from the center and four sides of the well at 20× magnification), and the percentages of cells with nuclear YAP1/TAZ were quantified by using ImageJ. At least 100 cells were counted in each experiment. The means ± SEM were calculated by using one-way ANOVA.

Bone histology and immunohistochemistry

Humeral bone tissue of neonates or femur tissue of adult mice were dissected, fixed (4 h at 4°C for neonatal bones, and overnight at 4°C for adult bones) in 4% paraformaldehyde, frozen or embedded in paraffin, and sectioned (5-µm thickness). Adult bones were decalcified in 10% EDTA solution at 4°C for 4 wk. The tissue sections were stained with hematoxylin and eosin by using a standard procedure. Immunohistochemical and immunofluorescent staining of tissue sections was performed as described previously (Wu et al., 2015) with mouse antibodies recognizing kindlin-2 (clone 3A3.5; Tu et al., 2003; Wu et al., 2015), YAP1/TAZ (sc-101199; Santa Cruz), or mouse IgG (Santa Cruz) as a control.

Images were acquired at room temperature by using a microscope (Eclipse Ni; Nikon) with Plan 10×/0.25 and Plan 20×/0.4 objectives (Nikon) equipped with a digital camera (DS-Fi1c; Nikon) and NIS-Elements F Ver4.30.01 image analysis software (Nikon).

In vivo analysis of MSC osteogenic and adipogenic differentiation capacities

For in vivo osteogenic differentiation, 2 × 10^6/ml hMSCs expressing GFP were embedded into matrix gels. HMSCs in matrix gels were induced with osteogenic medium for 3 d. The matrix plugs were then implanted subcutaneously into Nu/Nu mice. The specimens were dissected from the mouse recipients and analyzed 4 wk later (Tang et al., 2013).

Immunoprecipitation

hMSCs were harvested and homogenized in western and IP lysis buffer (P0013; Beyotime) supplemented with 1 mM PMSF (329-98-6; Sigma-Aldrich) for 30 min at 4°C and precleared with Protein A/G PLUS-Agarose (sc-2003; Santa Cruz) for 30 min. Immunoprecipitation was performed overnight at 4°C, with 2–3 mg protein lysate by using a mouse anti–kindlin-2 antibody (clone 3A3.5; Tu et al., 2003; Wu et al., 2015) or normal mouse IgG (sc-2025; Santa Cruz) as the control reaction. Proteins binding to the antibodies were then immunoprecipitated by incubation with Protein A/G PLUS-Agarose for 2 h, followed by washing once with lysis buffer and twice with PBS. The samples were then subjected to Western blotting by using mouse anti-MLCK (M7905; Sigma-Aldrich) and mouse anti–kindlin-2 (clone 3A3.5) antibodies.

Nano LC-MS/MS analysis

Nano LC–MS/MS was performed as we described previously (Sun et al., 2017). Briefly, hMSCs lysates were immunoprecipitated with mouse anti–kindlin-2 antibody (clone 3A3.5) or mouse control IgG (sc-2025; Santa Cruz). Each immunoprecipitated sample was then resolved in SDS loading buffer and denatured at 95°C for 5 min. After protein separation by 10% SDS-PAGE and staining with Brilliant Blue G-250, each lane of the gel was excised, cut into six slices, and incubated with 500 µl 50 mM ammonium bicarbonate (ABC) and 50% (vol/vol) acetonitrile (ACN) for destaining. The gel slices were dehydrated and rehydrated with 200 µl 100% ACN. Disulfide bonds were reduced with 200 µl 10 mM DTT. The proteins were alkylated with 100 mM iodoacetamide and 50 mM ABC for 30 min at room temperature in the dark. The gel pieces were dried in a speed vacuum and incubated overnight at 37°C with sequencing-grade modified trypsin (Promega) at an enzyme-to-protein ratio of 1:100 (wt/wt). The resulting peptides were extracted sequentially from the gel slices with 200 µl 25 mM ABC and 200 µl 5% (vol/vol) formic acid (FA) and 50% ACN by sonication for 20 min at each stage. After all supernatants were combined, the peptides were dried in a speed vacuum. The dried peptide mixtures were dissolved in 100 µl 1% FA and desalted by using homemade C18-StageTips, which were prepared as described previously (Rappsilber et al., 2007). Finally, the eluted peptide samples were lyophilized to dryness and redissolved in 10 µl 0.1% (vol/vol) FA in water for nano LC-MS/MS analysis. Peptide mixtures were analyzed by an Orbitrap Fusion mass spectrometer (Thermo Fisher Scientific) coupled with an Easy-nLC 1000 (Thermo Fisher Scientific) ultra-high-pressure liquid chromatography pump. The LC separation system consisted of a trap column (100 µm inside diameter × 4 cm) and an analytic column with integrated spray tip (75 µm inside diameter × 20 cm), both packed with 3 µm/120 Å Repro-Sil-Pur C_{18} resins (Dr. Maisch HPLC GmbH). The buffers used for separation were 0.1% FA in water and 0.1% FA in ACN. Half of the obtained samples were first loaded onto the trap column at a flow rate of 2 µl/min and then separated by the analytic column at a flow rate of 300 nl/min. The gradient was set as follows: from 3% to 7% ACN in 2 min, from 7% to 22% ACN in 50 min, from 22% to 35% ACN in 10 min, from 35% to 90% ACN in 2 min, holding at 90% ACN for 6 min, declining to 3% ACN in 2 min, and holding at 3% ACN for 13 min. Full MS scans were performed in an Orbitrap mass analyzer over m/z range of 350–1550 with a mass resolution of 120,000.

GST pull-down assays

For generation of GST fusion proteins containing WT or mutant forms of kindlin-2, the corresponding cDNA sequences were cloned into pGEX-4T-1 vectors. *Escherichia coli* strain BL21 were then transformed with the expression vectors. GST and GST-fusion proteins were purified from *E. coli* BL21 with Glutathione-Sepharose 4B matrix (GE Healthcare) by following the manufacturer's instructions. Purified proteins were resolved by SDS-PAGE to verify their size and purity. In pull-down assays, GST or GST-fusion proteins bound to Glutathione-Sepharose beads were incubated with hMSC lysates for 2 h at 4°C. The beads were washed three times with buffer (20 mM Tris, pH 7.5, 150 mM NaCl, and 0.1% Triton X-100) and analyzed by SDS-PAGE. Actin and MLCK were detected by Western blotting. GST-fusion proteins were detected by Coomassie blue staining.

Flow cytometric analysis of apoptosis and activation of integrin β1

Apoptosis was assessed by using a dead-cell apoptosis kit with Annexin V-FITC and propidium iodide (PI; Invitrogen) by following the manufacturer's instructions. Briefly, hMSCs (10^6; passage 8) were seeded in 6-cm dishes. The cells were then harvested, washed with cold PBS, resuspended in 100 µl of the incubation buffer containing 3 µl annexin-V-FITC labeling reagent, and 1 µl propidium iodide solution, and further incubated at room temperature for 15 min in the dark. Then, the cells were immediately analyzed by using a flow cytometer (Partec CyFlow). The total percentage of apoptosis was expressed as the sum of early and late apoptotic cell populations.

For analysis of integrin β1 activation, cells (as specified in each experiment) were analyzed by flow cytometry as previously described (Wang et al., 2015). In brief, cells were suspended in PBS containing 1% BSA at 10^6/ml. 100-µl cell aliquots were incubated with mouse antibodies specific for activated β1 integrin (HUTS-4, MAB2079Z; Millipore) and total β1 integrin (P4C10, MAB1987; Millipore) at room temperature for 30 min. The cells were then washed three times and incubated for 30 min at 4°C with Alexa Fluor 594-conjugated goat anti–mouse IgG secondary antibody (1:300; Abcam). After three washes, 10,000 events were determined by flow cytometry (Becton Dickinson,

http://www.bd.com) and analyzed by using FlowJo 7.6.1 software. The mean fluorescence intensities (MFI) were calculated using the CellQuest software. β1 integrin activation index equals the MFI of HUTS-4 staining divided by the MFI of P4C10 staining.

Analysis of RhoA activation by FRET

The RhoA sensor (Raichu-RhoA-CR) was a gift from M. Matsuda (Kyoto University, Kyoto, Japan; Aoki and Matsuda, 2009). In brief, enhanced yellow fluorescent protein and enhanced cyan fluorescent protein were replaced by Clover and mRuby2, respectively. The coding sequence of Clover-RhoA-PKN-mRuby2 was then subcloned into an adenoviral vector. hMSCs (passage 8) were infected with adenovirus expressing Clover-RhoA-RKN-Rubby and seeded onto a 10-ng/ul-fibronectin-coated Lab-TekR II chambered German cover glass system (Thermo Fisher Scientific) and grown overnight to confluence. Each plate containing cells was transferred to a temperature-controlled (37°C) imaging chamber. Time-lapse imaging data were acquired with Nikon eclipse Ti microscope with 20× objective at 1-min intervals by using the GFP and RFP channels (Lumencor LED) for advanced microscopy and cell imaging. For FRET analysis, images were cropped, background subtracted, and converted to 32-bit images. Further processing was done by smoothing both channels, thresholding the FRET channel, and finally converting the images to ratio images (FRET/clover) by using the analysis method described by Aoki and Matsuda (2009). Images were saved as TIFF files for presentation.

RhoA activity assay by G-LISA

RhoA activity was determined by using a Rho G-LISA RhoA Activation Assay kit (Biochem) by following the manufacturer's protocol (Cytoskeleton Inc.). The results were normalized to protein levels, which were measured by using the Precision Red protein assay reagent. Total RhoA was detected by Western blotting with a mouse anti-RhoA antibody (sc-418; Santa Cruz).

Preparation of polyacrylamide hydrogels with different stiffness

hMSCs were plated on Collagen-I–coated polyacrylamide hydrogels by following a previously described protocol (Wang and Pelham, 1998; Cretu et al., 2010). In brief, glass coverslips were activated successively with 100 mM NaOH for 5 min, 3-aminopropyltri-methoxysilane (281778; Sigma-Aldrich) for 5 min, and 0.5% glutaraldehyde (G7776; Sigma-Aldrich) for 30 min. Hydrogels of different stiffness (soft vs. stiff) were prepared with two prepolymer solutions containing different acrylamide/bis-acrylamide ratios. Specifically, hydrogels of soft substrate contained 10% acrylamide/0.026% bis-acrylamide, whereas hydrogels of stiff substrate contained 10% acrylamide/0.3% bis-acrylamide. The polyacrylamide sheets were assembled on the activated coverslips upon adding 0.5% ammonium persulfate (09830; Sigma-Aldrich) and 0.005% TEMED, and subsequently activated by incubation with 1 mM Sulfo-SANPAH (22589; Thermo Fisher Scientific) under 452 nm UV light for 5 min. The activated polyacrylamide sheets were then coated with 0.3 mg/ml Collagen-I at 4°C overnight before seeding with hMSCs at a density of 1.5×10^5 cells on each 7.5-cm coverslip.

Microcomputed tomography

Neonates were fixed overnight in 70% ethanol and analyzed by high-resolution microcomputed tomography (Skyscan1172; Bruker; Zhen et al., 2013). The scanner was set at a voltage of 60 kVp, a current of 100 µA and a resolution of 4.89 µm per pixel. Images were acquired with cooled charge-coupled device fiber-optically coupled to scintillator (11 Mp, 12 bit). PBS was used as the imaging medium. Images were reconstructed and analyzed by using NRecon v1.6 and CTAn v1.14, respectively. CTVox v3.0 software was used to visualize 3D models.

Statistical analysis

Results are presented as means ± SEM or percentages of population. Statistical analyses were performed by using GraphPad Prism 6.0. Data distribution was assumed to be normal, but this was not formally tested. One-way ANOVA with Tukey's multiple comparison test was used. A p-value <0.05 was considered significant.

Online supplemental material

Fig. S1 shows that the level of kindlin-2 is increased during MSC osteogenic differentiation and decreased during MSC adipogenic differentiation in vitro and in vivo. Fig. S2 shows that knockout of kindlin-2 in osteoblast progenitor cells causes severe limb shortening and defective osteogenesis. Fig. S3 shows the effect of kindlin-2 knockout on YAP1 expression. Fig. S4 shows subcellular localization of kindlin-2 LK/AA mutant in hMSCs. Figs. S5 and S6 show that kindlin-2 regulates MSC geometry and actin stress fiber formation. Fig. S7 shows kindlin-2 expression on micropatterned substrates. Table S1 shows the sequences of primers used for quantitative RT-PCR.

Acknowledgments

We thank Liu Xin for microcomputed tomography technical assistance, Dr. Ruijuen Tian for help with LC-MS/MS analysis, Dr. Michiyuki Matsuda for the Clover-RhoA-RKN-Rubby-FRET vector, and Drs. Jason D. Weber (Washington University, St. Louis, MO) and Yandong Zhang (Southern University of Science and Technology) for providing the pLVX vector.

This work was supported by the Chinese Ministry of Science and Technology grant 2016YFC1302100; the Science and Technology Innovation Committee of Shenzhen Municipality grants JCYJ20150831142427959 and ZDSYS20140509142721429; the National Natural Science of Foundation of China grants 81430068, 31471311, and 31401187; the Natural Science Foundation of Guangdong Province grants 2015A030313763 and 2017B030301018; and the National Institutes of Health grant AR068950.

The authors declare no competing financial interests.

Author contributions: L. Guo, T. Cai, K. Chen, R. Wang, J. Wang, C. Cui, J. Yuan, K. Zhang, and Z. Liu conducted the experiments. Y. Deng and G. Xiao contributed to the design of some of the experiments. L. Guo and C. Wu designed the experiments and wrote the paper.

Submitted: 25 December 2016
Revised: 22 October 2017
Accepted: 27 December 2017

References

Aoki, K., and M. Matsuda. 2009. Visualization of small GTPase activity with fluorescence resonance energy transfer-based biosensors. *Nat. Protoc.* 4:1623–1631. https://doi.org/10.1038/nprot.2009.175

Aragona, M., T. Panciera, A. Manfrin, S. Giulitti, F. Michielin, N. Elvassore, S. Dupont, and S. Piccolo. 2013. A mechanical checkpoint controls multicellular growth through YAP/TAZ regulation by actin-processing factors. *Cell.* 154:1047–1059. https://doi.org/10.1016/j.cell.2013.07.042

Bianco, P., M. Riminucci, S. Gronthos, and P.G. Robey. 2001. Bone marrow stromal stem cells: nature, biology, and potential applications. *Stem Cells.* 19:180–192. https://doi.org/10.1634/stemcells.19-3-180

Bledzka, K., K. Bialkowska, K. Sossey-Alaoui, J. Vaynberg, E. Pluskota, J. Qin, and E.F. Plow. 2016. Kindlin-2 directly binds actin and regulates integrin outside-in signaling. *J. Cell Biol.* 213:97–108. https://doi.org/10.1083/jcb.201501006

Bredella, M.A., M. Torriani, R.H. Ghomi, B.J. Thomas, D.J. Brick, A.V. Gerweck, C.J. Rosen, A. Klibanski, and K.K. Miller. 2011. Vertebral bone marrow fat is positively associated with visceral fat and inversely associated with IGF-1 in obese women. *Obesity (Silver Spring).* 19:49–53. https://doi.org/10.1038/oby.2010.106

Cao, J.J. 2011. Effects of obesity on bone metabolism. *J. Orthop. Surg. Res.* 6:30–36. https://doi.org/10.1186/1749-799X-6-30

Chen, Q., P. Shou, C. Zheng, M. Jiang, G. Cao, Q. Yang, J. Cao, N. Xie, T. Velletri, X. Zhang, et al. 2016. Fate decision of mesenchymal stem cells: adipocytes or osteoblasts? *Cell Death Differ.* 23:1128–1139. https://doi.org/10.1038/cdd.2015.168

Cohen, A., D.W. Dempster, E.M. Stein, T.L. Nickolas, H. Zhou, D.J. McMahon, R. Müller, T. Kohler, A. Zwahlen, J.M. Lappe, et al. 2012. Increased marrow adiposity in premenopausal women with idiopathic osteoporosis. *J. Clin. Endocrinol. Metab.* 97:2782–2791. https://doi.org/10.1210/jc.2012-1477

Connelly, J.T., J.E. Gautrot, B. Trappmann, D.W. Tan, G. Donati, W.T. Huck, and F.M. Watt. 2010. Actin and serum response factor transduce physical cues from the microenvironment to regulate epidermal stem cell fate decisions. *Nat. Cell Biol.* 12:711–718. https://doi.org/10.1038/ncb2074

Cretekos, C.J., Y. Wang, E.D. Green, J.F. Martin, J.J. Rasweiler IV, and R.R. Behringer. 2008. Regulatory divergence modifies limb length between mammals. *Genes Dev.* 22:141–151. https://doi.org/10.1101/gad.1620408

Cretu, A., P. Castagnino, and R. Assoian. 2010. Studying the effects of matrix stiffness on cellular function using acrylamide-based hydrogels. *J. Vis. Exp.* 10:1472–1476.

Dowling, J.J., E. Gibbs, M. Russell, D. Goldman, J. Minarcik, J.A. Golden, and E.L. Feldman. 2008. Kindlin-2 is an essential component of intercalated discs and is required for vertebrate cardiac structure and function. *Circ. Res.* 102:423–431. https://doi.org/10.1161/CIRCRESAHA.107.161489

Dupont, S. 2016. Role of YAP/TAZ in cell-matrix adhesion-mediated signalling and mechanotransduction. *Exp. Cell Res.* 343:42–53. https://doi.org/10.1016/j.yexcr.2015.10.034

Dupont, S., L. Morsut, M. Aragona, E. Enzo, S. Giulitti, M. Cordenonsi, F. Zanconato, J. Le Digabel, M. Forcato, S. Bicciato, et al. 2011. Role of YAP/TAZ in mechanotransduction. *Nature.* 474:179–183. https://doi.org/10.1038/nature10137

Engler, A.J., S. Sen, H.L. Sweeney, and D.E. Discher. 2006. Matrix elasticity directs stem cell lineage specification. *Cell.* 126:677–689. https://doi.org/10.1016/j.cell.2006.06.044

Fukuchi, Y., H. Nakajima, D. Sugiyama, I. Hirose, T. Kitamura, and K. Tsuji. 2004. Human placenta-derived cells have mesenchymal stem/progenitor cell potential. *Stem Cells.* 22:649–658. https://doi.org/10.1634/stemcells.22-5-649

Georgiou, K.R., S.K. Hui, and C.J. Xian. 2012. Regulatory pathways associated with bone loss and bone marrow adiposity caused by aging, chemotherapy, glucocorticoid therapy and radiotherapy. *Am. J. Stem Cells.* 1:205–224.

Goeckeler, Z.M., and R.B. Wysolmerski. 1995. Myosin light chain kinase-regulated endothelial cell contraction: The relationship between isometric tension, actin polymerization, and myosin phosphorylation. *J. Cell Biol.* 130:613–627. https://doi.org/10.1083/jcb.130.3.613

Gregorieff, A., Y. Liu, M.R. Inanlou, Y. Khomchuk, and J.L. Wrana. 2015. Yap-dependent reprogramming of Lgr5(+) stem cells drives intestinal regeneration and cancer. *Nature.* 526:715–718. https://doi.org/10.1038/nature15382

Guo, L., Y. Zhou, S. Wang, and Y. Wu. 2014. Epigenetic changes of mesenchymal stem cells in three-dimensional (3D) spheroids. *J. Cell. Mol. Med.* 18:2009–2019. https://doi.org/10.1111/jcmm.12336

Halder, G., S. Dupont, and S. Piccolo. 2012. Transduction of mechanical and cytoskeletal cues by YAP and TAZ. *Nat. Rev. Mol. Cell Biol.* 13:591–600. https://doi.org/10.1038/nrm3416

Hao, J., Y. Zhang, Y. Wang, R. Ye, J. Qiu, Z. Zhao, and J. Li. 2014. Role of extracellular matrix and YAP/TAZ in cell fate determination. *Cell. Signal.* 26:186–191. https://doi.org/10.1016/j.cellsig.2013.11.006

Hao, Y., A. Chun, K. Cheung, B. Rashidi, and X. Yang. 2008. Tumor suppressor LATS1 is a negative regulator of oncogene YAP. *J. Biol. Chem.* 283:5496–5509. https://doi.org/10.1074/jbc.M709037200

Hiemer, S.E., and X. Varelas. 2013. Stem cell regulation by the Hippo pathway. *Biochim. Biophys. Acta.* 1830:2323–2334. https://doi.org/10.1016/j.bbagen.2012.07.005

Hong, A.W., Z. Meng, and K.L. Guan. 2016. The Hippo pathway in intestinal regeneration and disease. *Nat. Rev. Gastroenterol. Hepatol.* 13:324–337. https://doi.org/10.1038/nrgastro.2016.59

Jaalouk, D.E., and J. Lammerding. 2009. Mechanotransduction gone awry. *Nat. Rev. Mol. Cell Biol.* 10:63–73. https://doi.org/10.1038/nrm2597

James, A.W. 2013. Review of signaling pathways governing MSC osteogenic and adipogenic differentiation. *Scientifica (Cairo).* 2013:684736–684752.

Jiang, X., M. Ye, X. Jiang, G. Liu, S. Feng, L. Cui, and H. Zou. 2007. Method development of efficient protein extraction in bone tissue for proteome analysis. *J. Proteome Res.* 6:2287–2294. https://doi.org/10.1021/pr070056t

Jing, H., L. Liao, Y. An, X. Su, S. Liu, Y. Shuai, X. Zhang, and Y. Jin. 2016. Suppression of EZH2 prevents the shift of osteoporotic MSC fate to adipocyte and enhances bone formation during osteoporosis. *Mol. Ther.* 24:217–229. https://doi.org/10.1038/mt.2015.152

Justesen, J., K. Stenderup, E.N. Ebbesen, L. Mosekilde, T. Steiniche, and M. Kassem. 2001. Adipocyte tissue volume in bone marrow is increased with aging and in patients with osteoporosis. *Biogerontology.* 2:165–171. https://doi.org/10.1023/A:1011513223894

Karystinou, A., A.J. Roelofs, A. Neve, F.P. Cantatore, H. Wackerhage, and C. De Bari. 2015. Yes-associated protein (YAP) is a negative regulator of chondrogenesis in mesenchymal stem cells. *Arthritis Res. Ther.* 17:147–160. https://doi.org/10.1186/s13075-015-0639-9

Larjava, H., E.F. Plow, and C. Wu. 2008. Kindlins: Essential regulators of integrin signalling and cell-matrix adhesion. *EMBO Rep.* 9:1203–1208. https://doi.org/10.1038/embor.2008.202

Li, C., G. Zhen, Y. Chai, L. Xie, J.L. Crane, E. Farber, C.R. Farber, X. Luo, P. Gao, X. Cao, and M. Wan. 2016. RhoA determines lineage fate of mesenchymal stem cells by modulating CTGF-VEGF complex in extracellular matrix. *Nat. Commun.* 7:11455–11469. https://doi.org/10.1038/ncomms11455

Li, H., Y. Deng, K. Sun, H. Yang, J. Liu, M. Wang, Z. Zhang, J. Lin, C. Wu, Z. Wei, and C. Yu. 2017. Structural basis of kindlin-mediated integrin recognition and activation. *Proc. Natl. Acad. Sci. USA.* 114:9349–9354. https://doi.org/10.1073/pnas.1703064114

Li, Z., C. Liu, Z. Xie, P. Song, R.C. Zhao, L. Guo, Z. Liu, and Y. Wu. 2011. Epigenetic dysregulation in mesenchymal stem cell aging and spontaneous differentiation. *PLoS One.* 6:e20526–e20534. https://doi.org/10.1371/journal.pone.0020526

Lv, H., L. Li, M. Sun, Y. Zhang, L. Chen, Y. Rong, and Y. Li. 2015. Mechanism of regulation of stem cell differentiation by matrix stiffness. *Stem Cell Res. Ther.* 6:103–113. https://doi.org/10.1186/s13287-015-0083-4

Ma, Y.Q., J. Qin, C. Wu, and E.F. Plow. 2008. Kindlin-2 (Mig-2): A co-activator of β3 integrins. *J. Cell Biol.* 181:439–446. https://doi.org/10.1083/jcb.200710196

Mammoto, A., and D.E. Ingber. 2009. Cytoskeletal control of growth and cell fate switching. *Curr. Opin. Cell Biol.* 21:864–870. https://doi.org/10.1016/j.ceb.2009.08.001

McBeath, R., D.M. Pirone, C.M. Nelson, K. Bhadriraju, and C.S. Chen. 2004. Cell shape, cytoskeletal tension, and RhoA regulate stem cell lineage commitment. *Dev. Cell.* 6:483–495. https://doi.org/10.1016/S1534-5807(04)00075-9

Misra, M., and A. Klibanski. 2013. Anorexia nervosa, obesity and bone metabolism. *Pediatr. Endocrinol. Rev.* 11:21–33.

Moerman, E.J., K. Teng, D.A. Lipschitz, and B. Lecka-Czernik. 2004. Aging activates adipogenic and suppresses osteogenic programs in mesenchymal marrow stroma/stem cells: The role of PPAR-gamma2 transcription factor and TGF-beta/BMP signaling pathways. *Aging Cell.* 3:379–389. https://doi.org/10.1111/j.1474-9728.2004.00127.x

Montanez, E., S. Ussar, M. Schifferer, M. Bösl, R. Zent, M. Moser, and R. Fässler. 2008. Kindlin-2 controls bidirectional signaling of integrins. *Genes Dev.* 22:1325–1330. https://doi.org/10.1101/gad.469408

Moroishi, T., C.G. Hansen, and K.L. Guan. 2015. The emerging roles of YAP and TAZ in cancer. *Nat. Rev. Cancer.* 15:73–79. https://doi.org/10.1038/nrc3876

Oka, T., V. Mazack, and M. Sudol. 2008. Mst2 and Lats kinases regulate apoptotic function of Yes kinase-associated protein (YAP). *J. Biol. Chem.* 283:27534–27546. https://doi.org/10.1074/jbc.M804380200

Qu, H., Y. Tu, X. Shi, H. Larjava, M.A. Saleem, S.J. Shattil, K. Fukuda, J. Qin, M. Kretzler, and C. Wu. 2011. Kindlin-2 regulates podocyte adhesion and fibronectin matrix deposition through interactions with phosphoinositides and integrins. *J. Cell Sci.* 124:879–891. https://doi.org/10.1242/jcs.076976

Qu, H., Y. Tu, J.L. Guan, G. Xiao, and C. Wu. 2014. Kindlin-2 tyrosine phosphorylation and interaction with Src serve as a regulatable switch in the integrin outside-in signaling circuit. *J. Biol. Chem.* 289:31001–31013. https://doi.org/10.1074/jbc.M114.580811

Rappsilber, J., M. Mann, and Y. Ishihama. 2007. Protocol for micro-purification, enrichment, pre-fractionation and storage of peptides for proteomics using StageTips. *Nat. Protoc.* 2:1896–1906. https://doi.org/10.1038/nprot.2007.261

Saltiel, A.R. 2003. Muscle or fat? Rho bridges the GAP. *Cell.* 113:144–145. https://doi.org/10.1016/S0092-8674(03)00277-0

Shi, X., Y.Q. Ma, Y. Tu, K. Chen, S. Wu, K. Fukuda, J. Qin, E.F. Plow, and C. Wu. 2007. The MIG-2/integrin interaction strengthens cell-matrix adhesion and modulates cell motility. *J. Biol. Chem.* 282:20455–20466. https://doi.org/10.1074/jbc.M611680200

Sordella, R., W. Jiang, G.C. Chen, M. Curto, and J. Settleman. 2003. Modulation of Rho GTPase signaling regulates a switch between adipogenesis and myogenesis. *Cell.* 113:147–158. https://doi.org/10.1016/S0092-8674(03)00271-X

Sun, Y., C. Guo, P. Ma, Y. Lai, F. Yang, J. Cai, Z. Cheng, K. Zhang, Z. Liu, Y. Tian, et al. 2017. Kindlin-2 association with Rho GDP-dissociation inhibitor α suppresses Rac1 activation and podocyte injury. *J. Am. Soc. Nephrol.* 28:3545–3562. https://doi.org/10.1681/ASN.2016091021

Tang, Y., R.G. Rowe, E.L. Botvinick, A. Kurup, A.J. Putnam, M. Seiki, V.M. Weaver, E.T. Keller, S. Goldstein, J. Dai, et al. 2013. MT1-MMP-dependent control of skeletal stem cell commitment via a β1-integrin/YAP/TAZ signaling axis. *Dev. Cell.* 25:402–416. https://doi.org/10.1016/j.devcel.2013.04.011

Tu, Y., S. Wu, X. Shi, K. Chen, and C. Wu. 2003. Migfilin and Mig-2 link focal adhesions to filamin and the actin cytoskeleton and function in cell shape modulation. *Cell.* 113:37–47. https://doi.org/10.1016/S0092-8674(03)00163-6

Valenti, M.T., L. Dalle Carbonare, and M. Mottes. 2016. Osteogenic differentiation in healthy and pathological conditions. *Int. J. Mol. Sci.* 18:41–50. https://doi.org/10.3390/ijms18010041

Wang, Y.L., and R.J. Pelham Jr. 1998. Preparation of a flexible, porous polyacrylamide substrate for mechanical studies of cultured cells. *Methods Enzymol.* 298:489–496. https://doi.org/10.1016/S0076-6879(98)98041-7

Wang, S., L. Guo, J. Ge, L. Yu, T. Cai, R. Tian, Y. Jiang, R.Ch. Zhao, and Y. Wu. 2015. Excess integrins cause lung entrapment of mesenchymal stem cells. *Stem Cells.* 33:3315–3326. https://doi.org/10.1002/stem.2087

Watt, F.M., and B.L. Hogan. 2000. Out of Eden: Stem cells and their niches. *Science.* 287:1427–1430. https://doi.org/10.1126/science.287.5457.1427

Wozniak, M.A., and C.S. Chen. 2009. Mechanotransduction in development: A growing role for contractility. *Nat. Rev. Mol. Cell Biol.* 10:34–43. https://doi.org/10.1038/nrm2592

Wu, C., H. Jiao, Y. Lai, W. Zheng, K. Chen, H. Qu, W. Deng, P. Song, K. Zhu, H. Cao, et al. 2015. Kindlin-2 controls TGF-β signalling and Sox9 expression to regulate chondrogenesis. *Nat. Commun.* 6:7531–7543. https://doi.org/10.1038/ncomms8531

Wu, Y., L. Chen, P.G. Scott, and E.E. Tredget. 2007. Mesenchymal stem cells enhance wound healing through differentiation and angiogenesis. *Stem Cells.* 25:2648–2659. https://doi.org/10.1634/stemcells.2007-0226

Wu, Y., R.C. Zhao, and E.E. Tredget. 2010. Concise review: Bone marrow-derived stem/progenitor cells in cutaneous repair and regeneration. *Stem Cells.* 28:905–915.

Zhang, J., G.A. Smolen, and D.A. Haber. 2008. Negative regulation of YAP by LATS1 underscores evolutionary conservation of the Drosophila Hippo pathway. *Cancer Res.* 68:2789–2794. https://doi.org/10.1158/0008-5472.CAN-07-6205

Zhao, B., L. Li, K. Tumaneng, C.Y. Wang, and K.L. Guan. 2010. A coordinated phosphorylation by Lats and CK1 regulates YAP stability through SCF(beta-TRCP). *Genes Dev.* 24:72–85. https://doi.org/10.1101/gad.1843810

Zhen, G., C. Wen, X. Jia, Y. Li, J.L. Crane, S.C. Mears, F.B. Askin, F.J. Frassica, W. Chang, J. Yao, et al. 2013. Inhibition of TGF-β signaling in mesenchymal stem cells of subchondral bone attenuates osteoarthritis. *Nat. Med.* 19:704–712. https://doi.org/10.1038/nm.3143

Zhong, W., K. Tian, X. Zheng, L. Li, W. Zhang, S. Wang, and J. Qin. 2013. Mesenchymal stem cell and chondrocyte fates in a multishear microdevice are regulated by Yes-associated protein. *Stem Cells Dev.* 22:2083–2093. https://doi.org/10.1089/scd.2012.0685